

**Aus der Radiologischen Universitätsklinik Tübingen  
Abteilung für Diagnostische und Interventionelle Neuroradiologie  
Ärztliche Direktorin: Professor Dr. U. Ernemann**

**Development of Functional Magnetic Resonance Imaging  
Method for the Examination of Subcortical Activation After  
Application of Auditory Stimuli**

**Inaugural-Dissertation  
zur Erlangung des Doktorgrades  
der Humanwissenschaften**

**der Medizinischen Fakultät  
der Eberhard Karls Universität  
zu Tübingen**

**vorgelegt von  
Michalina Ryn  
aus  
Tychy, Polen  
2014**

Dekan: Dr. I. B. Autenrieth

1. Berichterstatter: Professor Dr. U. Klose
2. Berichterstatter: Professor Dr. D. Kern

## TABLE OF CONTENTS

---

|   |    |
|---|----|
| SUMMARY .....   | 7  |
| ZUSAMMENFASSUNG.....  | 9  |
| 1. INTRODUCTION.....  | 11 |
| 1.1. AIM OF STUDY .....   | 11 |
| 2. THEORY.....  | 13 |
| 2.1. PHYSICAL PRINCIPLES OF MAGNETIC RESONANCE IMAGING .....                                | 13 |
| 2.1.1 ECHO PLANAR IMAGING .....   | 16 |
| 2.2. FUNCTIONAL MAGNETIC RESONANCE IMAGING (fMRI) .....                                     | 17 |
| 2.2.1 BOLD CONTRAST.....  | 18 |
| 2.3. ANATOMY OF THE AUDITORY PATHWAY .....  | 20 |
| 2.4. AUDITORY fMRI .....  | 21 |
| 2.4.1 WHY THIS TECHNIQUE IS SO IMPORTANT TO DEVELOP? .....                                  | 21 |
| 2.4.2 ISSUES ON BRAINSTEM fMRI.....   | 22 |
| 3. METHODS.....   | 25 |
| 3.1. MATERIALS AND METHODS - STANDARD PROTOCOL.....   | 25 |
| 3.1.1 SUBJECTS.....   | 25 |
| 3.1.2 EXPERIMENTAL DESIGN.....  | 25 |
| 3.1.3 AUDITORY STIMULI.....   | 26 |
| 3.1.4 DATA ACQUISITION .....  | 28 |
| 3.1.5 DATA ANALYSIS .....   | 28 |
| 3.2. STRATEGIES FOR IMPROVING THE DETECTION OF fMRI ACTIVATION IN<br>AUDITORY PATHWAY ..... | 30 |
| 3.2.1 CARDIAC GATED AND NON-GATED MEASUREMENTS .....  | 30 |
| 3.2.2 OPTIMIZATION THE TECHNICAL PARAMETERS .....   | 31 |
| 3.2.2.1 NUMBER OF SLICES .....  | 31 |

|         |   |    |
|---------|---|----|
| 3.2.2.2 | RESOLUTION .....  | 32 |
| 3.2.2.3 | MONAURAL STIMULATION .....  | 33 |
| 3.2.2.4 | fMRI ACTIVATION IN RELATION TO SOUND INTENSITY .....                            | 33 |
| 3.2.3   | FUNCTIONAL CONNECTION BETWEEN STRUCTURES IN AUDITORY PATHWAY .....              | 33 |
| 3.2.4   | INFLUENCE OF WHITE MATTER CORRECTION ON VISUALIZATION OF AUDITORY PATHWAY ..... | 35 |
| 3.2.5   | CHIRP STIMULI .....   | 37 |
| 3.2.6   | EFFECTS OF DIFFERENT TYPES OF AUDITORY STIMULI .....                            | 38 |
| 3.2.7   | INTERINDIVIDUAL STABILTY OF BRAINSTEM POSITIONS .....                           | 38 |
| 4.      | RESULTS.....  | 40 |
| 4.1.    | CARDIAC GATED AND NON-GATED MEASUREMENTS.....                                   | 40 |
| 4.2.    | OPTIMIZATION THE TECHNICAL PARAMETERS.....                                      | 45 |
| 4.2.1   | NUMBER OF SLICES .....  | 46 |
| 4.2.2   | RESOLUTION.....   | 46 |
| 4.2.3   | MONAURAL STIMULATION .....  | 48 |
| 4.2.4   | fMRI ACTIVATION IN RELATION TO SOUND INTENSITY .....                            | 50 |
| 4.3.    | FUNCTIONAL CONNECTION IN AUDITORY PATHWAY.....                                  | 51 |
| 4.4.    | INFLUENCE OF WHITE MATTER CORRECTION ON VISUALIZATION OF AUDITORY PATHWAY ..... | 56 |
| 4.5.    | CHIRP STIMULI .....   | 57 |
| 4.6.    | EFFECTS OF DIFFERENT TYPES OF AUDITORY STIMULI .....                            | 58 |
| 4.7.    | INTERINDIVIDUAL STABILITY OF BRAINSTEM POSITIONS .....                          | 62 |
| 5.      | DISCUSSION .....  | 64 |
| 5.1.    | OPTIMIZATION THE TECHNICAL PARAMETERS.....                                      | 64 |
| 5.2.    | DATA EVALUATION .....   | 65 |
| 5.3.    | EFFECT OF DIFFERENT AUDITORY STIMULATION .....                                  | 67 |
| 5.4.    | STABILITY OF PRESENTED METHOD.....  | 68 |
|         | REFERENCES.....   | 69 |

ACKNOWLEDGMENTS..... 75  
CURRICULUM VITAE ..... 76



## SUMMARY

---

Over the last years the focus of the technique of functional magnetic resonance imaging (fMRI), based on BOLD contrast, has rapidly changed from a technical perspective to wide clinical applications. Therefore it became a unique instrument which is used to identify specific brain areas showing activation during the performance of a task.

Nowadays there is large amount of detailed information concerning activation in auditory cortex and much less is known about the role of the subcortical structures of the auditory pathway, like cochlear nucleus, superior olivary complex, nuclei of lateral lemniscus, inferior colliculi, and medial geniculate body. They play an important role on auditory information processing. However, the functional imaging of these subcortical structures is still a methodological and technical challenge for specialists such as neuroscientists, physicists, engineers and clinicians. The major problems in visualization of subcortical structures are: a) brainstem motion caused by heart beat, blood flow, cerebrospinal fluid movement, b) small size of the nuclei, c) interference of a stimuli with the background scanner noise and d) habituation. Methods and tools for visualizing the brainstem have improved, but they are still inadequate for clinical studies and also for studies investigating healthy volunteers for the above mentioned reasons.

The aim of this thesis was to develop a reliable fMRI method which allows the investigation of brainstem nuclei and the auditory cortex during application of auditory stimuli. In the present study, supplementary approaches (cardiac gated measurements, functional connectivity analysis, white matter and repetition times (TR) corrections) were applied in order to achieve satisfactory and reliable results.

All measurements were carried out with 3T whole body MR scanner (TimTrio, Siemens, Erlangen, Germany). Neural activation was detected by BOLD differences using  $T2^*$ -weighted echo planar images (EPI). Anatomical images were acquired using a MPRAGE sequence. The paradigm consisted of a listening task in which sounds were presented binaurally or monaurally to healthy subjects. A standard "ON/OFF" block paradigm was used. Pre-processing for single subject analysis was conducted with SPM5 (<http://www.fil.ion.ucl.ac.uk>). All necessary software for additional pre-processing, post-processing steps and visualization was written with Matlab (Math Works, Natick, MA, USA).

Within this thesis an appropriate fMRI measurement sequence for visualization of auditory pathway and processing routines were developed. Furthermore, it was presented how to achieve the intended results in terms of optimizing the technical parameters such as number of slices, resolution and auditory stimuli. Data evaluation was improved using additional approaches such as cardiac gated measurements and functional connectivity analysis. It was also shown how to improve post-processing steps by including signal from white matter as an additional regressor in statistical analysis. Results demonstrated ability to apply different auditory stimulation: music, syllables, chirps and their effect on auditory cortex and subcortical structures. It was presented how to prove the stability of the method. The idea was to examine the interindividual differences regarding the spatial distribution of activated voxels in healthy subjects. Further the coordinates of activated nuclei were compared with previous studies and anatomical atlases.

In summary, the visualization of the functional areas in the auditory cortex and brainstem is possible with the fMRI technique as developed by this thesis. The stability of the approach presented in this study showed that fMRI may play an important role in clinical fMRI examination of the auditory system. The presented method can be used efficiently and allow to investigate the afferent auditory pathway in patients with hearing problems, i.e. hearing loss or tinnitus. Comparing the clinical data with results associated with healthy people can provide important information for further research or therapeutical approaches.



## ZUSAMMENFASSUNG

---

In den vergangenen Jahren hat sich der Schwerpunkt des Interesses an der Technik der funktionellen Kernspintomographie (fMRT) von technischen Aspekten auf eine breite klinische Anwendung verschoben. Es ist eine Methode, mit der man beschreiben kann, welche Hirnareale bei der Durchführung einer bestimmten Aufgabe beteiligt sind.

Hinsichtlich der Aktivierung des auditorischen Kortexes gibt es heute eine Fülle von Informationen. Weniger gut untersucht, jedoch nicht minder wichtig für die akustische Informationsverarbeitung, ist die Rolle der verschiedenen subkortikalen Strukturen der Hörbahn, wie des Nucleus cochlearis, des Nucleus olivus superior, des Lemniscus Lateralis, des Colliculus Inferior und des medialen geniculaten Körpers. Die funktionelle Bildgebung dieser subkortikalen Strukturen, insbesondere die Darstellung des Hirnstamms, ist jedoch nicht trivial und stellt hohe methodische und technische Herausforderungen an die Experimente. Die größten Probleme können wie folgt zusammengefasst werden: a) Bewegungsartefakte innerhalb des Hirnstamms, die durch den Herzschlag, Blutfluss und Liquorbewegungen ausgelöst werden, b) die geringe Größe der Nuclei, c) die Interferenz der auditiven Stimuli mit dem Hintergrundgeräusch des Scanners sowie d) Gewöhnungseffekte. Die Methoden und Techniken zur Visualisierung des Hirnstammes haben sich in den letzten Jahren zwar verbessert, sind jedoch für die Durchführung von Studien mit Patienten und gesunden Probanden aufgrund der oben aufgeführten Gründe immer noch unzureichend.

Das Ziel dieser Arbeit war es, eine zuverlässige fMRT-Methode zu entwickeln, die die funktionelle Bildgebung des Hirnstamms und des auditorischen Kortex während der Präsentation von auditiven Reizen ermöglicht. Um aussagekräftige und reliable Ergebnisse zu erzielen, wurde eine Reihe von neuen Verfahren angewendet (z.B. pulsgetriggerte Messungen und methodisch ausgefeilte Datenanalysen, s.u.).

Alle Messungen wurden mit einem 3T Ganzkörperscanner (TimTrio, Siemens, Erlangen, Deutschland) durchgeführt. Die funktionellen Bilder wurden mittels einer T2\* gewichteten EPI-Sequenz und die strukturellen Bilder wurden mit einer MPRAGE-Sequenz aufgenommen.

Während der fMRT-Messungen hörten die gesunden Probanden akustische Reize über Kopfhörer, die im Rahmen eines Standard On-/Off Blockdesign entweder binaural oder monaural dargeboten wurden. Die Datenvorverarbeitung der einzelnen Probanden wurde mit

SPM5 (<http://www.fil.ion.ucl.ac.uk>) durchgeführt. Die nötige Software für weitere Vor- und Nachbearbeitungsschritte sowie die Visualisierungstools wurden mit Matlab (Math Works, Natick, MA, USA) geschrieben.

Im Rahmen dieser Arbeit wurde eine fMRT-Messsequenz für eine bessere Visualisierung der Hörbahn sowie geeignete Verarbeitungsschritte entwickelt. Dies wurde durch die Optimierung technischer und methodischer Parameter, wie die Anzahl der aufgenommenen Schichten, die Auflösung und die Art der präsentierten Stimuli erreicht. Eine Verbesserung der Datenerhebung und -auswertung konnte durch pulsgetriggerte Messungen und funktionelle Konnektivitätsanalysen erreicht werden. Durch die Verwendung des Signals der weißen Substanz als zusätzlichen Regressor in die Datenanalyse konnte das Ergebnis verbessert werden. Weiterhin wurde gezeigt, dass es möglich ist, verschiedene akustische Reize zu präsentieren, denn Musik, Silben, Chirp waren mit Aktivierungen im akustischen Kortex und den subkortikalen Strukturen der Hörbahn assoziiert.

Es wurde gezeigt, wie man die Reliabilität der Methode überprüfen kann. Die Idee war, die interindividuellen Unterschiede hinsichtlich der räumlichen Verteilung der aktivierten Voxel bei gesunden Probanden zu untersuchen. Die Koordinaten der aktivierten Kerne wurden mit den Ergebnissen aus früheren Studien und anatomischen Atlanten verglichen.

Zusammengefasst kann festgehalten werden, dass die Darstellung der funktionellen Areale innerhalb des akustischen Kortex und Hirnstamm anhand der in dieser Arbeit entwickelten fMRT-Methode möglich ist. Die Robustheit des in der vorliegenden Studie durchgeführten Verfahrens zeigt, dass fMRT eine wichtige Bedeutung für die klinische Untersuchung des auditorischen Systems bekommen kann. Die hier vorgestellte Methode kann effizient angewendet werden und ermöglicht, die afferente Hörbahn in Patienten mit Hörstörungen (Hörverlust oder Tinnitus) zu untersuchen. Der Vergleich klinischer Daten mit den Ergebnissen von gesunden Probanden kann in Zukunft wichtige Informationen für weitere Forschungsschritte und eventuell auch Hinweise für mögliche therapeutische Maßnahmen liefern.

# 1. INTRODUCTION

---

## 1.1. AIM OF STUDY

Functional magnetic resonance imaging (fMRI) is a technique for measuring brain activity. This method offers many advantages like: it is noninvasive since it does not use ionizing radiation; it allows studying cortical activation induced by the various stimuli, functional maps can be generated with a spatial resolution of millimeters. In the past ten years the growth of fMRI based on research applications has been explosive. The range of fMRI experiments is increasing, what gives an opportunity to create more complicated questions concerning functions of the human brain. Currently also the development of fMRI in clinical applications is significant for a better diagnosis of various psychiatric and neurological disorders.

The main goal of this project was to develop an efficient, fast and stable fMRI method which allows the investigation of brainstem nuclei and auditory cortex after application of auditory stimuli. The desired measurement technique was used at first in a research project for the examination of properties of brainstem activations and in future it should be possible to use it also as a part of routine MR examination.

Within the desired measurement technique, the following steps were included:

1. Construction of the paradigm, length and kind of auditory stimuli, monaural or binaural stimulation
2. Optimization of the experimental parameters e.g., number of slices, resolution, sound intensity
3. Additional innovation such as cardiac gated measurements
4. Analysis of the experimental data: functional connections, influence of white matter correction
5. Inspection and verification of the stability of the presented technique

The work in this dissertation is organized as follows. Chapter 1 starts with an introduction of this work followed by summarization of the main contributions of this dissertation.

Chapter 2 (Theory), briefly describes the physical principles of magnetic resonance imaging, it includes explanation of echo planar imaging, BOLD contrast technique, anatomy of auditory pathway. It focuses also on the application of functional magnetic resonance imaging (fMRI) to the auditory system in the human brain, describes recent fMRI studies on the human central auditory pathway, emphasizing anatomical, methodological, technical issues, and applications to the brainstem.

Chapter 3 describes in detail materials and methods, concerning subjects who have participated in the study, auditory stimuli, experimental design, data acquisition and data analysis. This chapter focuses on the standard protocol used through this project and a short introduction of developments which were made during each part of the study. All the improvements were employed to get a fast and stable fMRI method to visualize the auditory pathway. Chapter 4 presents the results part which is divided into several sections. Chapter 5 (Discussion) describes the relationship, trends and generalizations among the results, significance of this work. It contains all possible results interpretations compared with other studies.

## 2. THEORY

---

The phenomenon of nuclear magnetic resonance (NMR) was for the first time demonstrated in 1945 by Purcell [1] and Bloch [2]. Seven years later these two scientists were awarded the Nobel Prize in physics for their discovery. With this discovery NMR has become an important analytical method of chemical composition and structures in biomedical science. About 23 years later (1973), imaging based on NMR was proposed by Lauterbur [3] and Mansfield [4]. Since then magnetic resonance imaging (MRI) has been one of the most widely used instrument in many biomedical, chemical and engineering applications.

This chapter will present the basic of MR imaging, short description of fast MRI sequence (echo planar imaging), basics of functional MRI including the physical and biophysical bases of the signal as well as knowledge of the auditory pathway and application of fMRI in auditory processing.

### 2.1. PHYSICAL PRINCIPLES OF MAGNETIC RESONANCE IMAGING

The quantum mechanical description of atomic nuclei predicts the property of spin angular momentum, which is characterized by:

$$J = \left(\frac{h}{2\pi}\right) \sqrt{I(I+1)}$$

where  $h$  is Planck's constant and  $I$  is the quantum spin number, which can be 0,  $\frac{1}{2}$ , 1, .... The orientation of the angular momentum is described by the second quantum number  $m$  ( $m=I, I-1, I-2 \dots -I$ ).

Nuclei of atoms exhibit proportionality between their total magnetic moment  $\mu$  and total angular momentum  $J$ . This relation is given by:

$$\mu = \gamma J$$

Where  $\gamma$  is the gyromagnetic ratio, which is a constant characteristic to each nucleus.

In presence of the magnetic field  $\vec{B}_0$  energy of the magnetic moment  $\vec{\mu}$  is given by:

$$E = -\vec{\mu}\vec{B}_0 = \gamma \left( \frac{h}{2\pi} \right) m \vec{B}_0$$

Among the most commonly used nuclei are  $^1\text{H}$ ,  $^{13}\text{C}$ ,  $^{19}\text{F}$ ,  $^{23}\text{Na}$  and  $^{31}\text{P}$ . For imaging in biological systems hydrogen is the most common, primarily due to its high concentration in human body and high sensitivity. For hydrogen the quantum spin number  $I$  is equal to  $\frac{1}{2}$ , therefore quantum number  $m$  can be  $\frac{1}{2}$  or  $-\frac{1}{2}$ . That represents the parallel and anti-parallel direction of the magnetic moment to the direction of the  $B_0$  field. As a consequence, there are two energy levels:

$$E_1 = \frac{1}{2} \gamma \left( \frac{h}{2\pi} \right) B_0$$

$$E_2 = -\frac{1}{2} \gamma \left( \frac{h}{2\pi} \right) B_0$$

This splitting of the energy levels is called the Zeemann effect.

Change in energy levels causes the absorption or emission of a photon. NMR absorption will occur when electromagnetic radiation of the correct frequency is applied to match the energy difference between these energy levels mentioned above. Since the energy of the electromagnetic pulse is described by its frequency ( $\hbar\omega$ ), the resonance condition is given by:

$$E_1 - E_2 = \Delta E = \hbar\omega = \gamma \left( \frac{h}{2\pi} \right) B_0$$

what give us Larmor equation:

$$\omega = \left( \frac{\gamma}{2\pi} \right) B_0$$

where  $\omega$  is resonance frequency (Larmor). The gyromagnetic ratio is constant for a given nucleus, thus the resonance frequency will only depend on the external magnetic field  $B_0$ .

In an external magnetic field  $B_0$  spins will be randomly distributed between parallel ( $N_{m-1}$ ) and anti-parallel ( $N_m$ ) states. Thus, the ratio between these energy states is given by the Boltzmann relation:

$$\frac{N_{m-1}}{N_m} = \exp\left(\frac{\Delta E}{kT}\right) = \exp\left(\frac{\hbar\omega}{kT}\right)$$

where  $k$  is the Boltzmann constant and  $T$  is the temperature.

An equal distribution of the spins between these two states will occur only for very high temperatures. At equilibrium, the net magnetization vector lies along the direction of the applied magnetic field  $B_0$  and is called the equilibrium magnetization  $M_0$ . For a typical temperature a small surplus of spins in parallel direction will create the macroscopic net magnetization  $M_z$  (longitudinal magnetization vector) parallel to the direction of the  $B_z$  magnetic field. Application of an RF pulse change the direction of net magnetization and then the transverse magnetization appears. The recovery of longitudinal magnetization is called  $T_1$  relaxation ('spin-lattice') and follows an exponential function described by a  $T_1$  time constant:

$$M_z = M_0 \left[ 1 - \exp\left(\frac{-t}{T_1}\right) \right]$$

The loss of net magnetization in the transverse plane (xy) is called  $T_2$  relaxation ('spin - spin') and is given by:

$$M_{xy} = M_0 \exp\left(\frac{-t}{T_2}\right)$$

When the RF pulse is turned off, the transverse component of magnetization vector produces an oscillating magnetic field which induces a current in the receiver coil. This is the free induction decay (FID) signal.

The inhomogenities in the static magnetic field and in the tissue cause the spins get out of phase faster than  $T_2$ . The time constant for the observed change of the signal is called the  $T_2^*$  relaxation and is described by:

$$M_{xy} = M_0 \exp\left(\frac{-t}{T_2^*}\right)$$

Effect of changing local magnetic field inhomogeneities ( $T_2^*$  weighted sequences) will be described in the next part of this dissertation.

### **2.1.1 ECHO PLANAR IMAGING**

Mansfield in 1977 proposed a very fast MR imaging sequence called echo planar imaging (EPI) [5, 6]. Among all of the existing MR sequences EPI nowadays is an often used one. Full image of a human brain can be acquired after just a single excitation pulse in only a fraction of second. EPI offers major advantages over conventional MR imaging such as decreased motion artifacts, reduced time of scanning and it offers the ability to image physiological processes of the human body. As a consequence this fast technique finds wide applications in clinical diagnosis and scientific investigation of dynamic brain function (functional magnetic resonance imaging, diffusion imaging, perfusion imaging, and cardiac imaging).

In echo planar imaging sequence, all the signal information needed to reconstruct the image is obtained after a single excitation pulse. The slice selection gradient and the RF pulse determine the location. The analysis of the spatial distribution of the spins along orthogonal directions in the selected slice has been solved by phase encoding gradient and readout gradient. Excited spins are dephased by an initial readout gradient. Reversion of the dephasing process is possible due to applying a readout gradient of opposite polarity resulting in the gradient echo. A train of echoes is generated by repeating this process. Signal intensity can decay to zero because of spin-spin relaxation ( $T_2$ ) and  $T_2^*$  effects (field inhomogeneity and magnetic susceptibility) [7]. The scheme of pulse sequence is presented in the Fig. 1.



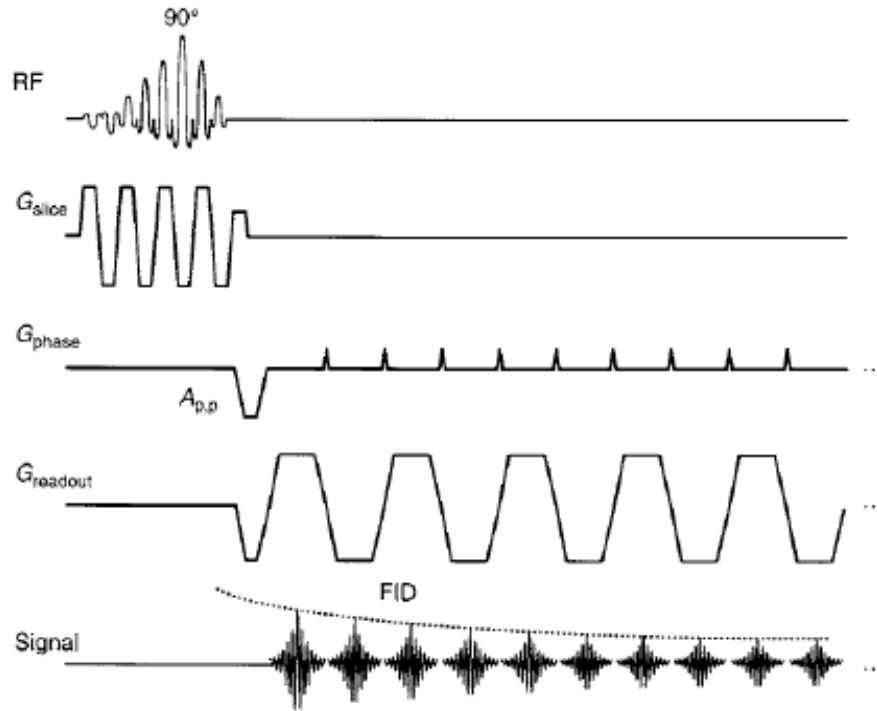


**Fig. 1; Pulse sequence diagram for gradient echo EPI [8].**

## 2.2. FUNCTIONAL MAGNETIC RESONANCE IMAGING (fMRI)

Functional magnetic resonance imaging (fMRI) is a widely used method which can detect discrete areas of slight perfusion changes within the brain resulting from neural activity in health and disease. Development in magnetic resonance imaging (MRI) has showed the possibility to map functional activity in human brain with good spatial and temporal resolution. Up to now the following fields have been investigated in healthy volunteers: vision [9], motor [10], language [11], emotion [12], memory [13], auditory [14] and pain [15]. However many studies have been also performed in patients within the fields of psychiatric disorders [16], epilepsy [17], stroke [18] and presurgical planning [19]. As we can see the application of the technique is commonly used in cognitive neuroscience and also starts to extend into clinical practice.

The most common method of fMRI is blood oxygenation level-dependent (BOLD) imaging. This effect depends on the ratio between diamagnetic oxyhemoglobin and paramagnetic deoxyhemoglobin of venous blood increase and results in a less tissue-blood susceptibility

difference. Ever since its discovery by Ogawa in 1990, the BOLD effect plays a dominant role in the field of fMRI [20-22].

### **2.2.1 BOLD CONTRAST**

As I mentioned above functional MRI based on the BOLD effect, which is a non-invasive method assess changes in neuronal activity. The brain has ongoing demands for energy, which is produced by chemical processes requiring glucose and oxygen. The neuronal activation causes an increase in regional cerebral blood flow (CBF) and the use of glucose. Blood contains hemoglobin which can be oxygenated and deoxygenated. Oxyhemoglobin and deoxyhemoglobin have different magnetic properties. Diamagnetic oxyhemoglobin has no permanent magnetic dipole moment (little influence on the local field). However deoxyhemoglobin is in a paramagnetic high-spin state. During activation concentration of deoxyhemoglobin is reduced thus a field inhomogeneity decreases and signal loss occurs in  $T_2^*$ -weighted sequence. These small signal changes occur in a range not greater than 1-5% [22]. This process is clearly presented in the Fig.2. Physiological explanations of the BOLD signal can be introduced by comparing theory with the amplitude and time course of the measured BOLD signal. The time course of the human BOLD response is often called the hemodynamic response function (HRF). HRF has three phases; initial dip (small decrease in image), overshoot (strong increase in local blood flow what results in a substantial local oversupply of oxygenated hemoglobin), and post-stimulus undershot (reduced MRI signal below the pre-stimulus baseline level). Figure 3 presents the idealized time course of the BOLD response.

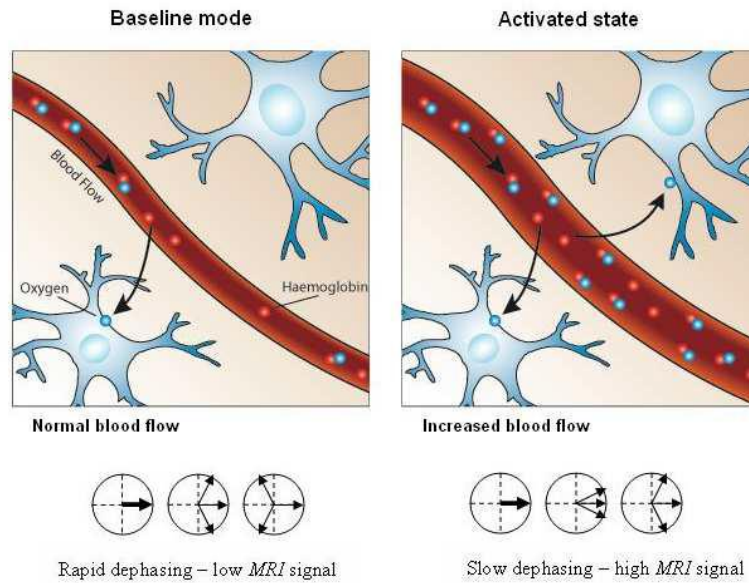


**Fig. 2;** If a cortical region is in baseline mode then neural activity is low and cerebral blood flow (CBF) is also at basal level. When hemoglobin is paramagnetic, it distorts the magnetic field. The hemoglobin involved in magnetic field inhomogeneity's leads to rapid dephasing of excited spins resulting in a low *MRI* signal level. However if the cortical region is in activated state, activity increases, leading to an increased CBF which is related to delivering oxygen. Since oxygenated hemoglobin doesn't significantly distort the homogeneity of the local magnetic field, excited spins dephase much slower than in the baseline state. As a result *MRI* signal is increased (BOLD effect) [23].

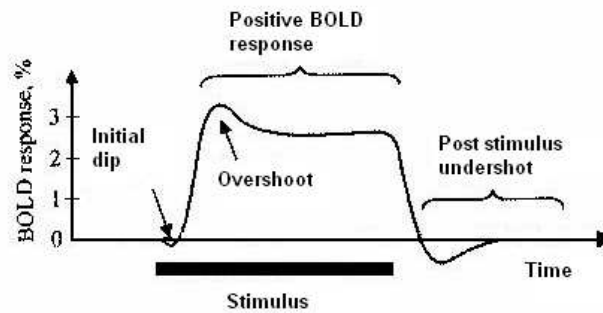


**Fig. 3;** Time course of the hemodynamic response function (HRF) [23].

### 2.3. ANATOMY OF THE AUDITORY PATHWAY

During hearing, activations are produced along the auditory pathway which includes several structures connected by ascending and descending white matter fibers. Group of nerve cells help to process and relay auditory information, encoded in the form of nerve impulses, directly to the highest cerebral levels in the cortex of the brain. The auditory pathway begins in the cochlear nucleus (CN), runs through superior olivary complex (SOC), nuclei of lateral lemniscus (nuclei of LL), inferior colliculi (IC), medial geniculate bodies (MGB) and ends in different parts of auditory cortex (Fig.4). Auditory areas consist of primary auditory cortex (anterior gyrus, Brodmann area 41), second auditory cortex (posterior gyrus, Brodmann area 42) and higher-order auditory cortex (Brodmann area 22).

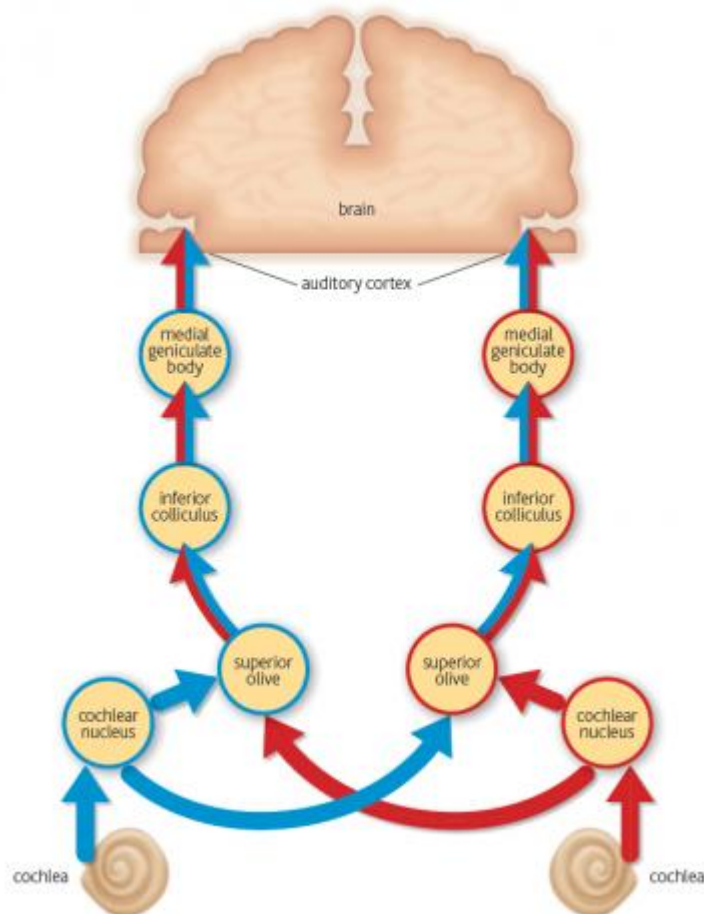


**Fig. 4; Schematic representation of auditory pathway [24].**

## **2.4. AUDITORY fMRI**

Nowadays functional resonance imaging gives us increasingly detailed information about the location of specific brain activity. The feasibility of fMRI to observe auditory cortex activation during a variety of listening tasks, including rhythm sequences, tone sequences, single words and tone intensity discrimination have been described by many authors [25, 26]. As well it has been shown that primary auditory cortex is functionally mapped in a tonotopic organization [27]. This task was methodologically challenging since scanner noise, frequency, intensity, type of auditory stimuli, time course of the paradigm and habituation could strongly influence the results or even mask the responses [28-30]. However rapid improvements in technology and methodology have had an enormous impact on solving these problems. Therefore activation in the auditory cortex during the presentation of auditory stimuli actually can be successfully performed by functional MR imaging (fMRI).

The growth of fMRI as a tool for studying auditory activation in the human brain gave the possibility to consider potentials for fMRI to visualize also other structures which take part in auditory processing. At the present time imaging the brainstem nuclei has been a unique challenge for neuroscientists, physicists, engineers, clinicians and image analysis specialists. In next section I will focus on recent studies on the human brainstem, methodological and technical issues to explain why fMRI of auditory pathway is still a great technical matter and why it is important to improve and develop this imaging method.

### **2.4.1 WHY THIS TECHNIQUE IS SO IMPORTANT TO DEVELOP?**

Brain is one of the most fascinating, complex and above all the most important organ. It works as the control center of the human body, receives information about the world around us from various senses such as seeing, hearing, smelling, tasting and touching. Thanks to fMRI we can study the function of the brain; we are able to distinguish whether it works properly or has some dysfunction. For this research the most interesting was the hearing sense and what is connected the auditory pathway.

All of the presented structures included in the auditory pathway play an important role in auditory information processing such as detection of sound intensity and left-right time differences as the basis of spatial mapping (SOC) [31]. MGB is responsible for relaying

frequency, intensity and binaural information, IC for mediating auditory gating processes and inhibitory neural transmission [32]. Nuclei of LL are sensitive to both timing and amplitude changes in sound and the role of CN is sound localization. These brainstem nuclei are constantly working together, so that our brain is able to process the auditory information into the central auditory cortex. However we can often meet with certain disabilities: hearing losses, tumors, and tinnitus. Why we need fMRI in this region? An fMRI efficient method should allow investigation of afferent auditory pathways in patients with hearing loss and tinnitus. *fMRI* technique can be useful for preoperative mapping and risk estimation. If a difference in fMRI activations between normal subjects and tinnitus can be shown, then this method can be used for control or different treatment approaches. Patients could be examined before, during and after different kinds of therapies and the comparison of the activation results could be used for an assessment whether the patients reaction approach that of normal subjects.

#### **2.4.2 ISSUES ON BRAINSTEM fMRI**

fMRI results within the subcortical structures such as CN, SOC, nuclei of LL, IC, MGB after acoustic stimulation are expected, but difficult to achieve. The major problems in visualization of brainstem nuclei are brainstem motion related to the heartbeat, blood flow, cerebrospinal fluid movement, small size of the nuclei, interference of stimuli with background scanner noise and habituation.

Previous studies in brain physiology reported that the images of human brain are hampered by dynamic changes during the fMRI experiment [33]. These physiological changes are due to fluctuations that can arise in heartbeat, cerebrospinal fluid movement and pulsation of arteries and veins located in different parts of the brain such as brainstem. Brainstem structures can move within the cardiac cycle up to several millimeters [34]. The mentioned signal changes were found to be the reason why fMRI in cognitive experiments can be less sensitive in brainstem than in cortex [35]. Several methods for the consideration of movement effects have been already implemented in fMRI measurements involving cardiac-gated measurements [36-39]. Guimaraes and colleagues showed that cardiac gated measurements improve the detection of brainstem activation, compared to measurements with constant TR. In these measurements, image acquisition is synchronized with the cardiac rhythm and the

influence of motion especially on the imaging of brainstem nuclei is reduced. As a consequence of the variable heart rate the interimage interval (TR) is no longer constant, which leads to signal variations based on a variable T1- relaxation. A correction for TR-dependent signal changes has to be performed [35]. One strategy for such a correction is fitting the signal time course in each voxel to a T1 saturation model [40]. This correction is rather time consuming. A less complex method is to use TR as an additional regressor in conventional SPM statistical analysis.

It is worth to remember that the size and morphology of these nuclei act against detecting their activation (cochlear nucleus is  $3 \times 3 \times 7 \text{ mm}^3$ , lateral lemniscus nucleus is  $2 \times 2 \times 5 \text{ mm}^3$ , superior olivary complex is  $2 \times 2 \times 5 \text{ mm}^3$  and inferior colliculus is  $6 \times 6 \times 4 \text{ mm}^3$ ) [41]. Therefore, the fMRI should be spatial smoothed by using Gaussian kernel smaller than usually used for larger cortical structures (8 mm).

Another source of artifacts is the interference of the background scanner noise in *fMRI* experiments. However, the problem may be reduced thanks to noise cancellation devices such as earplugs or headphones with insulated conducting tubes or by synchronizing the stimuli with the pulses of the *MR* sequences [28].

Also habituation can have influence on functional images. The reduction of activation after repeated stimuli during examination is an adaptive ability of subject to shield repetitive events in an environment [42].

Different types of the stimuli and different paradigms were used to obtain the activation of auditory brainstem nuclei. One of the studies reported subcortical activation in the auditory system using music with 100% and 75% detectability for IC and MGB respectively [35]. SOC (25%) and CN (31%) were detected using clicks [43]. In case of noise stimuli, SOC was detected with 84% and CN with 30% [44]. As we can see there is still missing information about other structures and also the percentage of detectability is not reasonable for use in clinical trials. Trying to solve the problems, one of the previous studies focuses on special paradigms. They used long, silent gaps lasting 10 seconds between acquisitions of successive fMRI volumes ("silent fMRI"). With success IC (94%), MGB (82%), SOC (82%) and CN (82%) were detected [45]. However, this technique is rather time-consuming and may be not suitable for clinical use. The paradigm used in another study [46] was more suitable for fast use in clinical environment. A conventional fMRI block design without use of special techniques like cardiac-gated fMRI was a rapid and reliable protocol applicable to patients with hearing abnormalities and tumors near the auditory subcortex.

The type and intensity of stimulus plays an important role in fMRI auditory brainstem activations. Experimental data show that the binaural response is smaller than the sum of monaural responses and even smaller than the contralateral monaural response alone. This process may be caused by a binaural inhibitory process or by the contributions from monaurally responsive neurons or neurons whose binaural responses are roughly equal to the sum of their monaural responses [44].

In summary, methods and tools for visualizing of the functional areas in brainstem have improved considerably over the last decades, but they are still inadequate not only for clinical studies but also studies with healthy volunteers. For most researchers the challenge is still largely unfulfilled and will require the development of truly integrated and highly useable tools.



### **3. METHODS**

---

#### **3.1. MATERIALS AND METHODS - STANDARD PROTOCOL**

First part of the chapter highlights the description of the standard protocol used throughout this project. It includes a description of the subjects who participated in the measurements, auditory stimuli, research design, data acquisition and data analysis. Innovation and additional developments will be presented in the second part.

##### **3.1.1 SUBJECTS**

This study used healthy human subjects as listeners in an fMRI experiment. All the participants were previously informed of the conditions of the study and gave written informed consent. The experiment was conducted according to the ethical guidelines and was approved by the local ethics committee.

47 healthy volunteers (31 females, 16 males, right handed, mean age  $27.5 \pm 5.1$  years, ranging from 22-46 years) without known auditory impairments, neurological diseases, implants or claustrophobia.

##### **3.1.2 EXPERIMENTAL DESIGN**

In all cases, a block design paradigm was used. Using that kind of experimental design, images have been acquired continuously during the epochs “ON” (sound stimulation) and epochs “OFF” (without stimulation). Afterwards the MRI signals are compared for the two types of blocks. The block design is simple to implement and can be used to localize several brain functions.

The block design paradigm in this study consisted of 7 stimulation cycles of 10 scans duration “ON” epochs (tones, rock or classical music, syllables, chirp) alternating with eight “OFF” epochs (10 scans) of no stimulation (Fig. 5). The duration of 10 scans depended on the cardiac rhythm (approximately 20 seconds). The ON block of pure tone stimuli consisted of 900 ms

beep followed by approximately 1100 ms silence, the real silence time was depended on the cardiac pulse. Auditory stimuli were synchronized with scanner work, thus each 2 seconds part of them started with a trigger pulse. One part of the music, syllables, and chirp was 2 seconds; consequently they were cut and the next part started if TR was shorter. If the TR was longer, there was a gap and the next part of stimuli started with the next TR. The gap was short and difficult to hear (length of 50 ms). Therefore the subjects heard the music, syllables and chirp as a continuous auditory stream. Participants were asked after scanning about the quality of the presented sound.

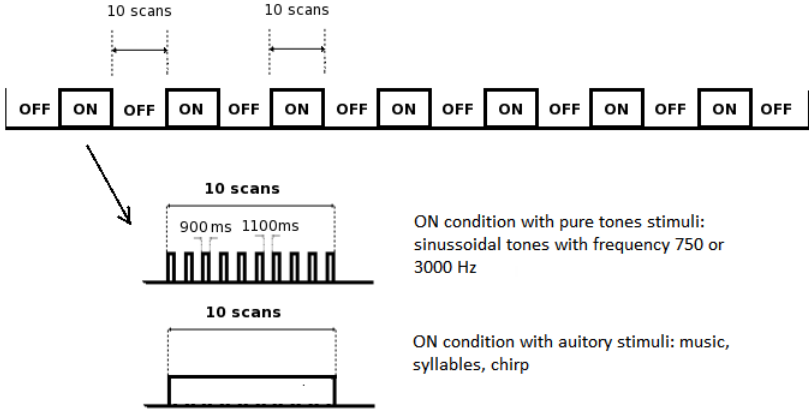


**Fig. 5; Block design paradigm.**

**3.1.3 AUDITORY STIMULI**

Six auditory stimuli were applied during different part of this study: single tones with frequencies of 750 and 3000 Hz, rock as well as classical music, syllables (“da-na”) and chirp stimuli. MR compatible headphones were used for presentation [47].

Pure sinusoidal digital tones with a duration of 900 ms were generated using the program Cool Edit Pro 2.0 (Adobe Systems Incorporated) and were stored as standard 16-bit uncompressed WAVE files with a sampling rate of 22050 Hz.

Music and syllables was cut into parts of 2 s in WavePad Sound Editor (NCH Swift Sound) and these were also stored as standard 16-bit uncompressed WAVE files with a sampling rate of 22050 Hz.

Chirp software version 2.1 was used to generate the waveform in ASCII format and then convert it to wav format 16 bits sampling rate 22050 Hz. A stimulus rate was 100hz then the

sound file was duplicate several times in order to increase the length to desired value (approximately 2 seconds).

All stimuli were presented binaurally, by playing the WAVE file with home written software on a computer with a commercial soundcard. The sound output was interfaced with a stereo integrated amplifier (Technics SU-VZ 320, Panasonic, Matsushita Electric Industrial CO. Osaka, Japan). The amplified sounds were delivered to the modified headphones (SENNHEISER HD 590-prestige, Wennebostel, Germany). The scheme of this additional equipment is presented in the Figure 6. Amplitude was adapted individually for each subject by presenting stimuli with different intensities to the subject during scanner operation. Each volunteer decided their individual volume amplitude that was most suitable for listening. Subjects were instructed to try to relax as much as possible, lay supine in the scanner with their eyes closed, motionlessly and pay attention to the music presented during scanning. All the experiments were performed in darkness.

Additionally to avoid the problem with attention, subjects had in the right hand the button box which was connected to the computer. They were asked to press one of the button using index finger, during each condition “OFF” and decided whether presented sound was the same as the sound from “ON” condition presented as a first one. Right button meant the sound was the same and left button different. The information about answer was stored in the computer, thus I was able to see if the participants focused on presented stimuli.

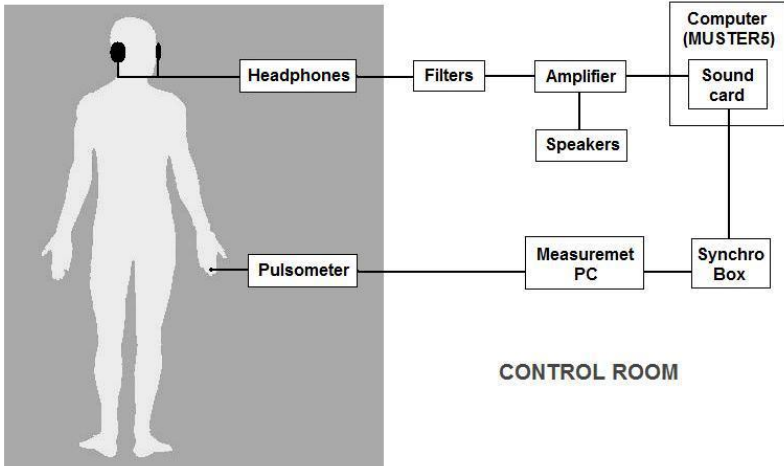
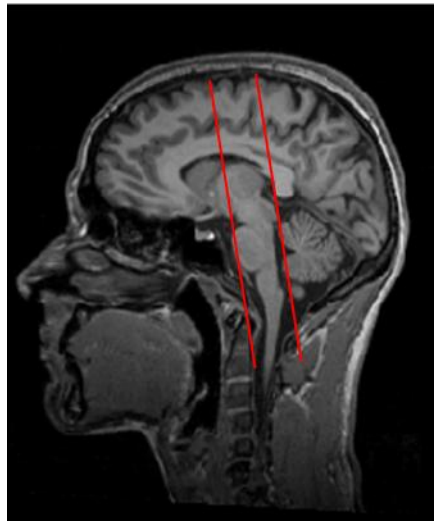


Fig. 6, Scheme of experimental equipment.

### 3.1.4 DATA ACQUISITION

Measurements were performed on a 3 Tesla MR whole body scanner (3T Trio Tim, Siemens, Erlangen, Germany) using a 12-channel head coil. EPI sequence was gated to the subject's pulse every second heartbeat, measured by finger pulse sensor situated on the left index finger. 153 images were acquired using an echo time (TE) of 30 ms; acquisition time (TA) of 607 ms; the repetition time depended on the cardiac rhythm. The volumes consisted of 10 slices with a slice thickness 2.5 mm with an inter slice gap of 0.5 mm, in plane resolution  $3 \times 3 \text{ mm}^2$  (64x64 matrix). These functional scans were positioned coronal to the brainstem (Fig.7). For each individual, *T1*- weighted structural images were acquired after *fMRI* data with a MPRAGE sequence (technical parameters as follows: TR= 2300 ms, TI= 1100 ms TE= 3.03 ms, flip angle=  $8^\circ$ , slice thickness= 1 mm, FoV=  $256 \times 256 \text{ mm}^2$ , and base resolution  $256 \times 256$ ). The functional data were superimposed on these anatomic references images after coregistration.



**Fig. 7; Orientation of acquired functional images.**

### 3.1.5 DATA ANALYSIS

Preprocessing of the functional images was carried out using Statistical Parametric Mapping software package (SPM5, <http://www.fil.ion.ucl.ac.uk>) and modified by home-written routines in Matlab (ver. 2010 *The MathWorks, Inc. Natick, MA, USA*). The functional time series were realigned; co-registered to the mean of the functional EPI images; and then

spatially normalized into a standard stereotaxic space using T1 template provided with SPM5 that is the MNI coordinate system. The normalized EPI images were subsampled to a voxel size of  $1 \times 1 \times 1 \text{ mm}^3$  and spatially smoothed with a Gaussian kernel of 6-mm full width at half maximum (FWHM). Pre-processing also included a segmentation of the anatomical structure data into three types of brain tissue: white matter (WM), grey matter (GM) and cerebro-spinal fluid (CSF).

Conventional functional block design analysis in individual subjects was performed using a general linear model (GLM). High pass filter is used to maximize the loss of noise and minimize the loss of signal. Slow signal drifts with a period longer than 120s were removed. Then first level ANOVA analysis was conducted with two different regressors; regressor of interest and nuisance regressors. The regressor of interest represented different levels of the experimental factor (ON and OFF conditions) and was calculated by convolving the box car function with the hemodynamic response function (HRF). Repetition times were used as a first nuisance regressor in the fMRI model specification, to account for signal variations based on the variable repetition times.

## 3.2. STRATEGIES FOR IMPROVING THE DETECTION OF fMRI ACTIVATION IN AUDITORY PATHWAY

Second part of the chapter is divided into several sections; each contains a short introduction of additional innovation concerning technical parameters, development for experimental data acquisition. All these innovative solutions were used to improve the visualization of the auditory pathway.

### 3.2.1 CARDIAC GATED AND NON-GATED MEASUREMENTS

It was mentioned in the introduction part, images of the human brain can be disrupted by signal changes and distortions during the course of the fMRI experiment. To avoid and minimize this effect we can use cardiac gated measurements. One consequence of this method is the effect of variable TR, due to heart rate variability. That is why it is worth to consider some additional steps in data analysis to reduce the influence of variable interscan intervals on functional images. Data can be analysed: without correction of signal intensity by using means TR, with correction; using exponential fitted curve or linear correction, using TR as a linear regressor. First method is simple however is not suggested due to variability of TR. T1 correction has been already described by many authors [35, 38, 48]. As was reported previously T1 was estimated by minimizing the variance in fitting an exponential T1 decay curve to fMRI signal intensity in each voxel to a model defined by:

$$S(TR) = M_0 \left[ \exp\left(\frac{-TR}{T_1}\right) \right]$$

Where S (TR) is signal intensity in voxel,  $M_0$  is maximal signal intensity in voxel, and TR is interscan interval (variable TR). Estimated  $M_0$  and T1 were used to correct S (TR) in each voxel to the average TR across all time points. Intensity of each voxel was corrected and all variations based on variable TR were eliminated. Corrected data series was then used to create functional maps using standard SPM procedures.

Third method is less complicated than exponential signal intensity correction; however it requires small variation of TR and linear behavior. This evaluation does not require additional

modeling of signal change, but to define in SPM the linear regressor which is equal real TR values. The real TR values are saved in report in home written software. Regressor is an additional column in the SPM design matrix and it includes the real values of TR, which model changes in signal intensity.

An fMRI data set can be presented as a set of voxels which corresponds to time points acquired during experiment. Thanks to statistical analysis it is possible to determine which voxel have a time course correlated to some experimental design. Time course can be estimated using statistical analysis (SPM). However, to get original time course from specific region, it is also possible to use some home written routines.

This section is divided into three parts. In the first one the aim was to show how signal intensity depends on different repetition times and which signal intensity correction is useful in data analysis. One healthy volunteer (man, 23 years old) was examined using gated measurements with six different mean TR. Auditory stimuli consisted of rock music.

The second part employed fMRI to measure activity in auditory cortex and brainstem using non-gated and gated measurements. I intend to check the influence of cardiac gated measurements in the level of auditory pathway and if it is necessary to use it in the further examination. Third part includes analysis of time courses after gated and non-gated experiments. A total of eight (seven females and one male) healthy, right handed volunteers participated in these experiments. They ranged in age from 22-36 years ( $27.5 \pm 5.4$  years). Repetition time for non-gated measurements was 2 seconds, and for gated depended on the cardiac cycle (mean TR about 2 seconds). Auditory stimuli consisted of rock music.

## **3.2.2 OPTIMIZATION THE TECHNICAL PARAMETERS**

### **3.2.2.1 NUMBER OF SLICES**

Starting with fMRI experiments it is important to carefully plan and modify research design. Most importantly is: what do we hope to find, which brain regions? Therefore, we have to decide how much of the brain image we want to get, what is related with number of the slices. Due to some limitation such as artifacts connected with fluctuating heart beat in some brain regions, number of slices has to be reduced. Due to limitation, an acquisition time is shorter for volume with less slices and this can reflect on the synchronization of image with cardiac

phase. Within this section the main issue was to check if it is important for brainstem visualization to reduce the number of slice.

Measurements were realized with cardiac gated method for three, right handed females ( $27.2 \pm 5.8$  years old, range 22-36). Two experiments were carried out: first with 32 slices (slice thickness 3.2 mm), covering the whole brain and the second one, with 10 slices (slice thickness 2.5 mm) positioned along the brainstem. Figure 8 presents scheme of cardiac phase.



**Fig. 8; Scheme of cardiac phase during acquisition with 32 and 10 slices.**

Three subjects were examined with two kinds of stimuli rock music and tones (3000 Hz). A total of six sessions were carried out during these two experiments (three for each).

### **3.2.2.2 RESOLUTION**

The small size of the nuclei play important role in fMRI studies of auditory pathway. One solution is using size of Gaussian kernel (6 mm). It was previous showed that this size of Gaussian kernel is appropriate. However we can also increase resolution of the fMRI image. Will give us better results? Answer for this question can be found in this section.

Eight healthy, right handed volunteers participated in the study (six females, two males, age range 22-34 years). Auditory stimuli consisted of rock and classical music. Two experiments with different resolution were performed. In both of them volumes consisted of 10 slices. In the first experiment slice thickness was 2.5 mm, in plane resolution of  $3 \times 3 \text{ mm}^2$ , base resolution  $64 \times 64$  and  $TE=30 \text{ ms}$ . In second one slice thickness 2.5 mm and in plane resolution  $2.5 \times 2.5 \text{ mm}^2$  (base resolution  $96 \times 96$ ,  $TE=34 \text{ ms}$ ) were used.



### **3.2.2.3 MONAURAL STIMULATION**

Contralaterality is the way the auditory cortex receives information predominantly from the contralateral ear. Lateralization refers to the dominance of one hemisphere in regard to a specific function [28]. Within this study fMRI was used to study contralaterality in the cortical processing of monaural sounds. In addition, I wanted to check how well fMRI corresponds to the assumption of contralaterality in auditory pathway.

Three healthy, right handed females participated in the study (age range 22-44 years). Auditory stimuli consisted of classical music. Stimulus was presented monaurally, by playing in one session just into right ears and in the second session just to left ear.

### **3.2.2.4 fMRI ACTIVATION IN RELATION TO SOUND INTENSITY**

In spite of fast growing research in the field of fMRI, there is still not much information about how sound is processed by the brain and how various sound aspects such as sound level are neutrally represented [48]. It has been shown that activation increases with increasing sound level in the auditory cortex [49], as well as at lower part of the auditory pathway [50].

In this study, auditory pathway was studied with two different amplitude of the sound. Standard one, adapted individually for each subject. Volunteer decided their individual volume of amplitude that was most suitable for listening. The second amplitude was reduced by about quarter in comparison to standard one.

This study was performed with 13 right handed volunteers (seven females and six males, age range 22-44 years,  $28.25 \pm 5.71$ ). Rock and classical music were presented to the subjects ears.

### **3.2.3 FUNCTIONAL CONNECTION BETWEEN STRUCTURES IN AUDITORY PATHWAY**

Most of previous reports presenting detection of subcortical and cortical structures used a conventional t-test analysis based on a block design of the stimulus. However, it is worth considering that fluctuations in signal intensity may also represent stimulus independent

changes in local blood flow at various times which might be similar in functionally connected brain areas [34]. Synchrony changes in signal intensity, metabolic rate and blood flow may be caused by neural connections between different functional parts of the brain [51] and can offer an improved detectability of subcortical activations. Functionally related and interconnected regions can be identified by functional connection analysis after resting state measurements and visualized using activation maps. This method presented in activation maps provides the similarity between a chosen reference area and signal in pixel with high t-value. Functional connectivity maps can characterize the relationship of the neural network in more detail and can play a role in understanding brain function [52].

Connections between selected areas have also been examined in fMRI measurements using specific stimuli such as motor tasks [53], auditory and visual [54] stimuli. In this case activation maps can be created similar as in resting state studies [55]. If the seed voxel is chosen at a known location of task activation, connectivity maps show the similarity of the signal intensity course between this region and all other voxels in the brain. Using this approach, voxels in auditory or visual areas have shown a significant correlation between the left and right hemispheres [54].

It can be assumed that those brainstem nuclei which are involved in processing of auditory signals have also a similar signal intensity time course from the auditory cortex. The goal of present section was to determine the activation in auditory cortex after application of acoustic stimuli and to identify the subcortical activations by functional connectivity analysis with the seed region in the auditory cortex.

Eight healthy volunteers (seven females, one male, right handed, mean age 27.5 years, ranging from 22-36 years) participated in this study. Two auditory stimuli were applied: rock as well as classical music. Overall, 10 sessions with cardiac gated measurements were carried out in eight volunteers (five sessions for rock and classical music). All imaging was performed with the standard parameters.

After conventional t-test block design analysis using the HRF as reference function, an analysis of functional connections was performed. Coordinates of the seed regions were chosen in the t-test analysis from the highest t-value in the auditory cortex on each side. The signal intensities in all measured volumes at the seed voxel built the reference time course, which was used as a regressor in first-level statistical analysis in SPM5. The resulting activation map voxels were superimposed onto anatomical images after application of a threshold of  $p < 0.001$  uncorrected. Only regions corresponding to areas within the brainstem

were taken into consideration. The positions of subcortical structures were identified on the basis of anatomical atlases.

### **3.2.4 INFLUENCE OF WHITE MATTER CORRECTION ON VISUALIZATION OF AUDITORY PATHWAY**

The blood oxygenation level dependent (BOLD) signal in fMRI experiments is not the only source for signal differences during a specific stimulation. Global effects in whole brain due to respiration can interfere with the localized BOLD effect especially within the brainstem. One strategy to minimize this effect is the correction for changes that are measurable within the whole white matter. An approach that considers white matter signal variations may allow removing global signal variations and increase the sensitivity of fMRI in regions of interest [56].

The objective of this study was to investigate the human subcortical and cortical areas during acoustical stimulation, using an additional step in statistical analysis. To improve the detection of brainstem nuclei and quality of t-maps the evaluated signal time course of the whole white matter was used as an additional regressor in statistical analysis. However in this section are presented also results for evaluations without any nuisance regressor, single nuisance regressor (TR), single nuisance regressor (WM) and both nuisances regressors (TR and WM). 24 healthy, right-handed subjects (15 females and nine male, age range: 24-46 years mean age  $29.1 \pm 4.2$ ) took part in the experiment.

Prior to statistical analysis, a white matter (WM) mask was created using Image Calculator in SPM5. Masks with three different thresholds were created (Fig.9). To minimize partial volume effect and to guarantee the highest probability that only signal from white matter was taken into consideration, then mask with the highest threshold (TH=0.99) was choose in further analysis.

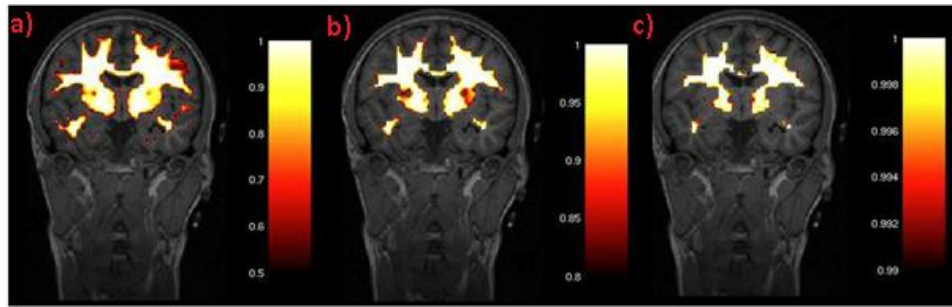


Fig. 9; White matter masks with different thresholds: TH=0.5 (a), TH=0.8 (b) and TH=0.99 (c).

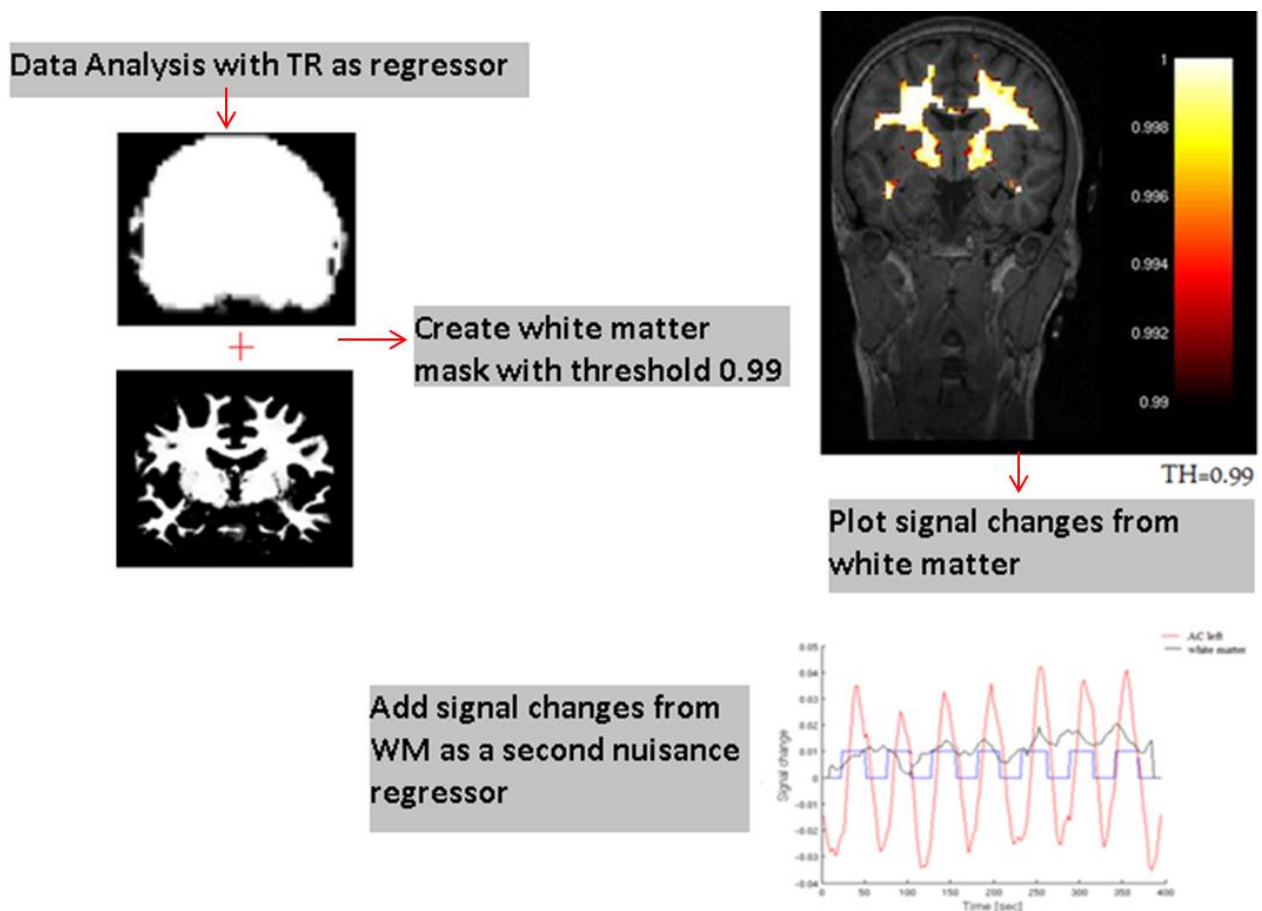


Fig. 10; Scheme illustrating data analysis with white matter as a regressor.

For each subject the average signal from the whole white matter was calculated individually. The whole process for data analysis with additional nuisance regressor is presented in Figure 10. Statistical data analysis in individual subjects was performed in four different ways:

1. Standard one, using one regressor of interest and any nuisance regressors
2. Using one regressor of interest and one nuisance regressor (TR)
3. Using one regressor of interest and one nuisance regressor (WM)
4. Using one regressor of interest and two nuisance regressors (TR and WM)

As was mentioned before nuisance regressors were used in fMRI model specification . To further improve the quality of the results, the average signal from white matter was used as the second nuisance regressor.

### 3.2.5 CHIRP STIMULI

The chirp is a special auditory acoustics stimulus that compensates the delay of the cochlea, related to the traveling wave. It compensates the basilar membrane (BM) temporal dispersion. When a transient stimulus progresses apical along the BM, single-unit activity is less synchronous with the preceding activity from basal units [57]. The chirp stimulus is a sound waveform in which the high-frequency components are delayed relative to the low-frequency components in appropriate amount (Fig.11).

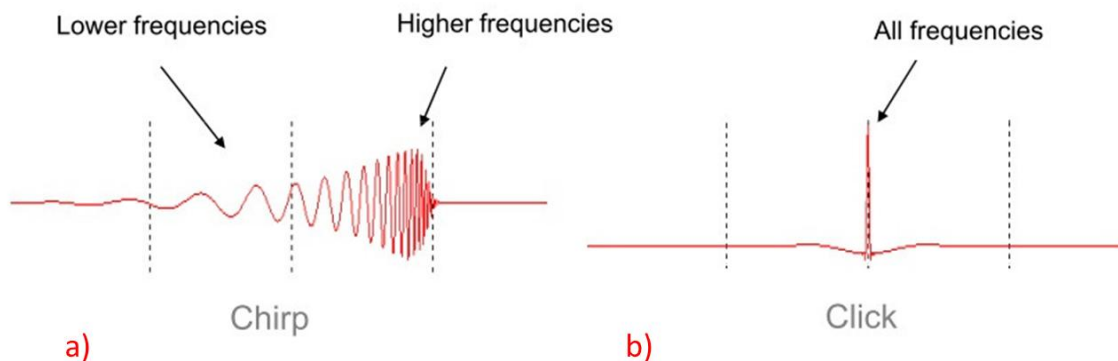


**Fig. 11; Temporal waveform of the broadband chirp stimuli (a) and click (b).**

These broad band stimuli with tonotopic temporal delay, not only, increase neural synchrony at peripheral and central levels, but also increase the neural activity in the brainstem. A chirp stimulus is commonly used in Auditory Brainstem Responses (ABR). The results shows that the signal amplitude of chirp-ABRs is two times larger compared to click-ABRs. This means

that there are more neurons activated at same time [58]. Up till now there are no studies which used this kind of stimulus for visualization of auditory pathway.

The question for this section was: what kind of effect on auditory brainstem has binaural chirp stimuli? Can we expect similar results like for Auditory Brainstem Responses?

10 healthy, right handed subjects (six females and four males, mean age  $25.7 \pm 4.1$ , ranging from 19-33 years,) were examined.

### **3.2.6 EFFECTS OF DIFFERENT TYPES OF AUDITORY STIMULI**

A total of 10 healthy subjects (six females and four males, mean age  $25.7 \pm 4.1$ , ranging from 19-33 years,) participated in the experiment. Auditory stimuli consisted of rock and classical music, syllables (“da-na”) and chirp.

The aim of this section was to check the influence of different auditory stimuli on auditory cortex and brainstem nuclei.

### **3.2.7 INTERINDIVIDUAL STABILITY OF BRAINSTEM POSITION**

From the previous experience we know how difficult visualization of the auditor pathway is. The present research was designed to develop an efficient, fast and stable method which in the future will be suitable for clinical use. How can we be sure if our method is appropriate and will give good results? One idea to prove it is inspection of the stability of individual activated positions within a group of healthy subjects and compare the coordinates of activated nuclei with previous studies and anatomical atlases.

The method was tested on 24, right-handed volunteers (15 females and nine male, age range: 24-46 years mean age  $29.1 \pm 4.2$ ). The acoustical stimulation consisted of rock and classical music.

The statistical data resulted in volume data set (x, y, z positions) containing t-values. All local maxima from this data set were calculated and listed with t-values and coordinates. To asses activation in subcortical regions, I defined regions of interest by using a sphere (6 mm diameter) that included CN (MNI-coordinates  $\pm 10, -38, -45$ ), SOC (MNI-coordinates  $\pm 13, 35,$

-41), IC (MNI-coordinates  $\pm 6, -33, -11$ ) and MGB (MNI-coordinates  $\pm 17, -24, -5$ ). The functional localization was based on the knowledge from previous studies and anatomical atlases [44, 59, 60]. Regions of interest are illustrated in Figure 12. Additionally, regions where CN and SOC overlap to each other were defined. First, from the list of local maxima, the voxels with the highest t-value and coordinates matching to the region of MGB and IC were selected. Then, I excluded from the list of local maxima overlapping area and we search maximum just for the regions of CN and SOC. If it was possible, I selected two different local maxima (coordinates match to region of CN and SOC). All local maxima were used to investigate the interindividual stability of the acoustic pathway nuclei positions.

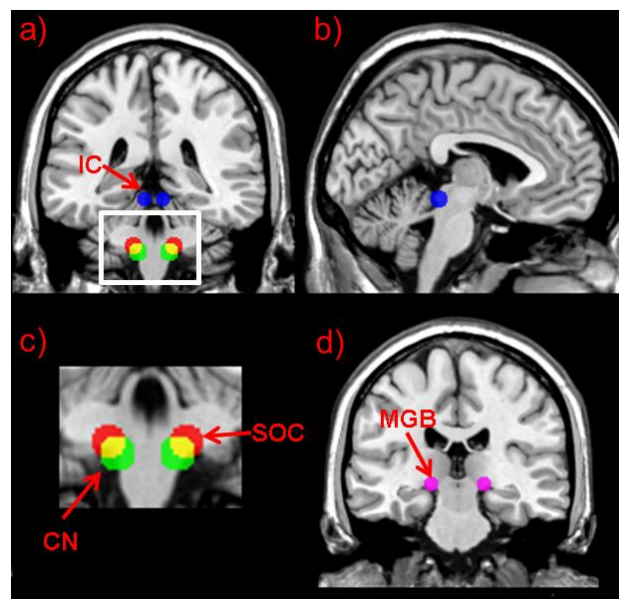


**Fig. 12; Regions of interest: : IC (blue), SOC (green), CN (red), overlap area of two nuclei SOC and CN (yellow) presented in coronal plane (a, c), IC (blue) in sagittal plane (b) and MGB (violet) in coronal plane (d). The overlap area (yellow) was excluded and we were interested only in founding local maxima for the CN (red) and SOC (green) region.**

## 4. RESULTS

---

### 4.1. CARDIAC GATED AND NON-GATED MEASUREMENTS

According to introduction from Chapter 3.2.1 concerning gated and non-gated measurements, experiment with six different TRs was performed to show signal intensity in dependency on repetition time for selected voxel. The plot (Fig.13) shows that the linear regression for correction of variable TR is adequate to change of signal (fMRI with cardiac gated measurements). Results showed that if TR is long enough (e.g., 8-10 seconds) then reach nearly full T1 relaxation in each measurement and correction can be omitted. As we can observe in most cases it is enough to use TR as a linear regressor due to small variations of TR (less than 10%) and dependency of signal intensity on repetition time was almost linear. However for the fourth experiment, large standard deviation of TRs occurs and therefore T1 correction using exponential curve fitting should be applied. Data analysis without and with corrections were performed for short and long TR. Results (Fig.14) showed that for the shorter TR without any correction only few voxels were activated in auditory cortex, however using linear and exponential correction auditory cortex was significantly activated. For both corrections similar results were obtained. Therefore for further data analysis; I decided to use less complicated linear correction. In case of longer TR both analysis showed similar results.

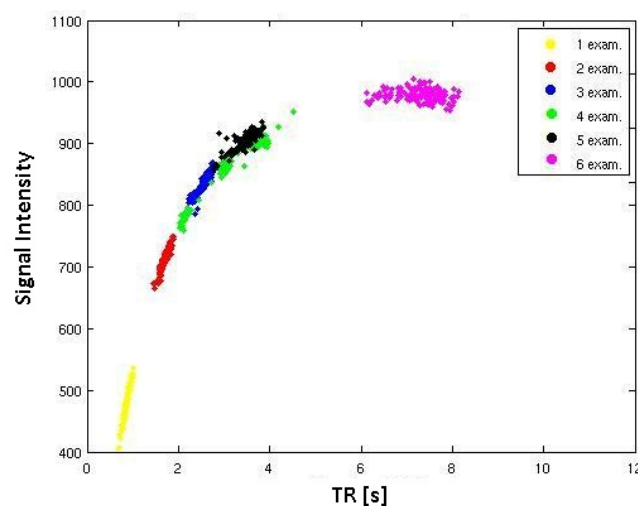


**Fig. 13; Signal intensity dependence of repetition time. Each color described examination with different TRs:  $0.86 \text{ s} \pm 4.7\%$  (yellow),  $1.70 \text{ s} \pm 5.3\%$  (red),  $2.60 \text{ s} \pm 4.7\%$  (blue),  $3.13 \text{ s} \pm 21.3\%$  (green),  $3.48 \text{ s} \pm 6.6\%$  (black), and  $7.29 \text{ s} \pm 7.5\%$  (purple).**



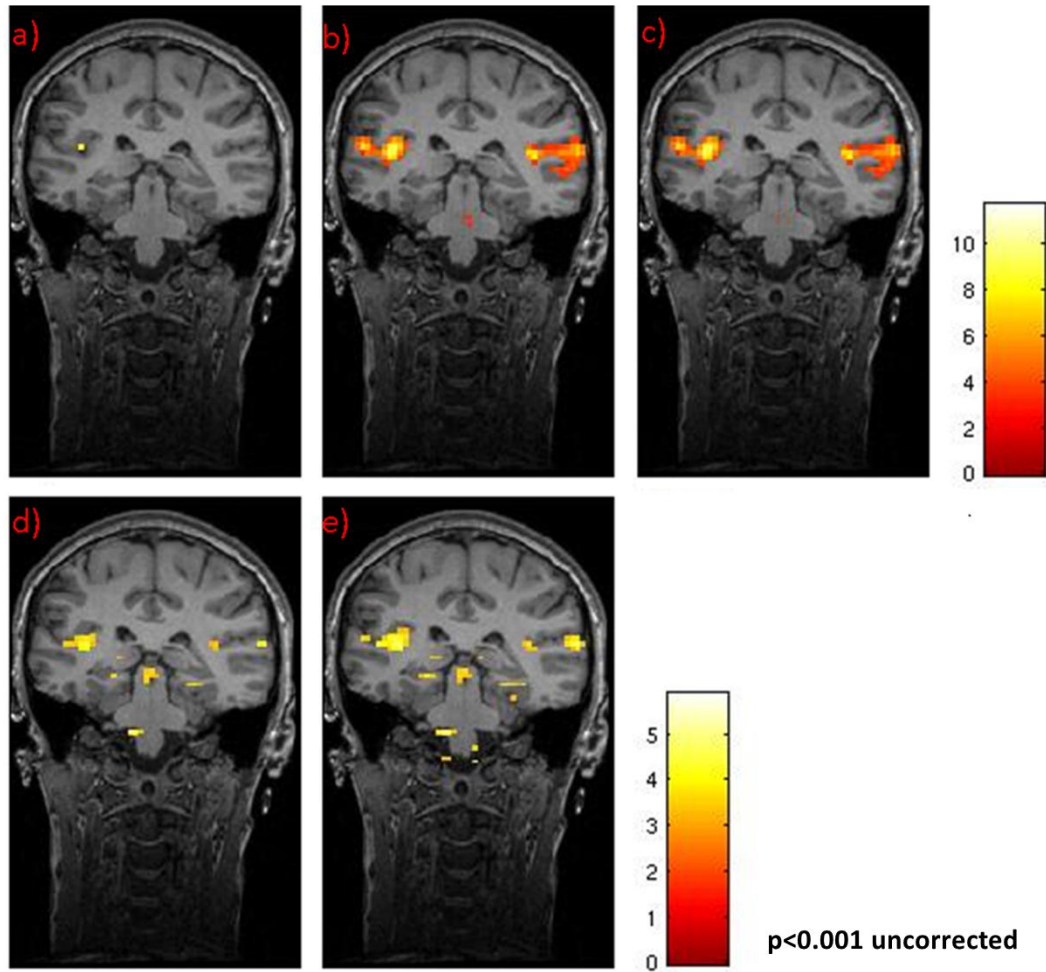


**Fig. 14;** T maps for cardiac gated measurements. TR=2.60 s: without correction (a), with linear correction (b) and with exponential curve fitting correction (c). Long TR (7.29 s) without any correction (d) and with linear correction (e).

The aim of the second part of this section was to determine the influence of gated and non-gated measurements on auditory cortex and brainstem. For gated measurements with linear correction and without it a single subject's analysis showed that auditory cortex was significantly activated in all individuals with the threshold of  $p < 0.001$  uncorrected (Fig. 15). Results without any correction for cardiac gated method showed that correction is necessary to improve the results. That is why for further analysis only data with correction was used. The t-values for cardiac gated method were more than two times higher than for none gated. Table 1 presents the t-values for each subject for both kinds of measurements.

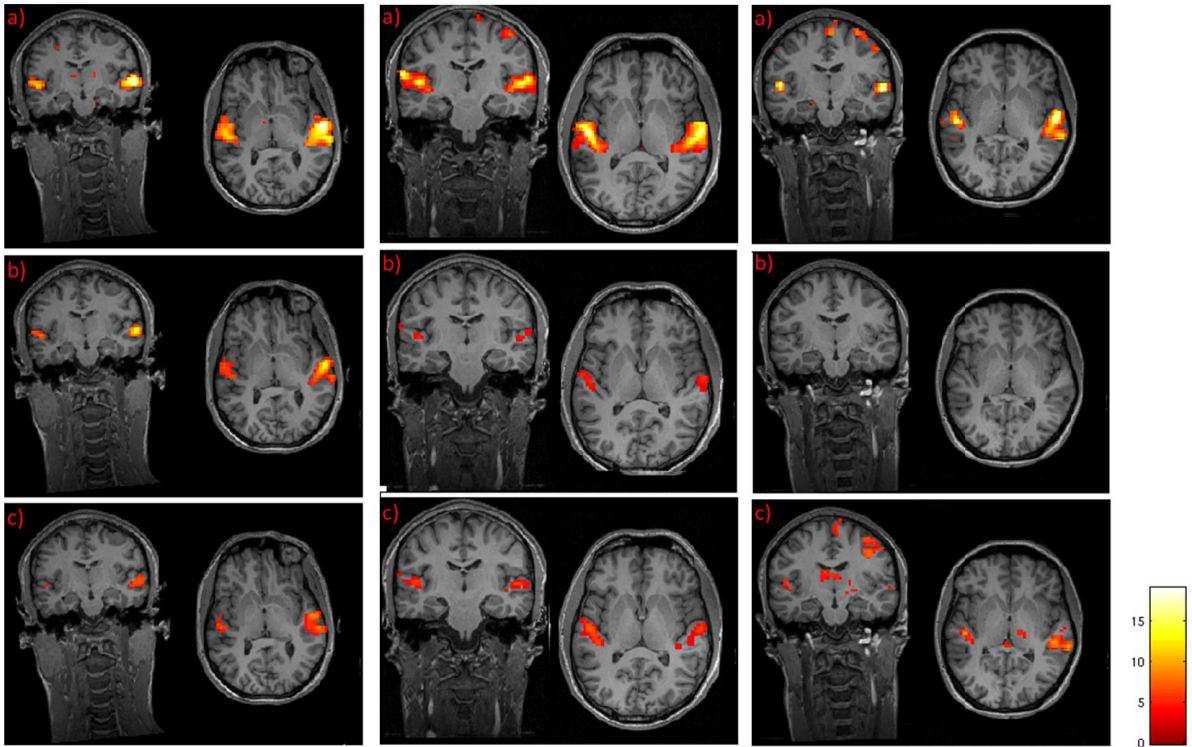


**Fig. 15; Visualization of auditory cortex for gated (a), none gated measurements (b) and gated without correction (c) for three different subjects.**

**Tab. 1; Local maxima in the region of right and left auditory cortex identified in standard t-test analysis for gated and none-gated measurements. T-values obtained for eight volunteers with the threshold of  $p < 0.001$  uncorrected.**

| Nr.                  | None-gated measurements |                  | Gated measurements |                   |
|----------------------|-------------------------|------------------|--------------------|-------------------|
|                      | Right                   | Left             | Right              | Left              |
| 1.                   | 4.88                    | 5.77             | 18.39              | 13.16             |
| 2.                   | 6.48                    | 5.21             | 13.9               | 9.74              |
| 3.                   | 6.32                    | 7.35             | 18.92              | 17.79             |
| 4.                   | 5.65                    | 7.46             | 13.51              | 11.73             |
| 5.                   | 8.55                    | 8.2              | 14.51              | 12.8              |
| 6.                   | 4.56                    | 5.24             | 14.56              | 15.45             |
| 7.                   | 7.45                    | 7.01             | 17.21              | 17.12             |
| 8.                   | 6.21                    | 5.99             | 17.54              | 16.52             |
| <b>Mean t-values</b> | <b>6.26±1.30</b>        | <b>6.53±1.12</b> | <b>16.07±2.17</b>  | <b>14.29±2.86</b> |

Subcortical auditory activation was examined in the following structures: cochlear nucleus, superior olivary complex, inferior colliculus and medial geniculate body (threshold  $p < 0.001$  uncorrected). In contrast to cardiac gated measurements no activation could be detected in expected brainstem areas for none-gated experiments and gated without correction. In Table 2 the number of identified subcortical activations and their t-values are displayed for both types of measurements. Figure 16 presents the anatomical regions of activated structures in brainstem area.

**Tab. 2; Mean t-values for both hemispheres obtained for auditory pathway: cochlear nucleus (CN), superior olivary complex (SOC), inferior colliculi (IC), medial geniculate body (MGB) and auditory cortex (AC) with threshold of  $p < 0.001$  uncorrected (eight volunteers).**

| Brain Region | None-gated measurements |            | Gated measurements |             |
|--------------|-------------------------|------------|--------------------|-------------|
|              | Right                   | Left       | Right              | Left        |
| AC           | 6.26 (8/8)              | 6.53 (8/8) | 16.07 (8/8)        | 14.29 (8/8) |
| MGB          | -                       | -          | 3.15 (5/8)         | 3.57 (5/8)  |
| IC           | -                       | -          | 5.32 (4/8)         | 4.50 (3/8)  |
| SOC          | -                       | -          | 2.01 (2/8)         | 2.81 (2/8)  |
| CN           | -                       | -          | 2.86 (4/8)         | 3.01 (5/8)  |

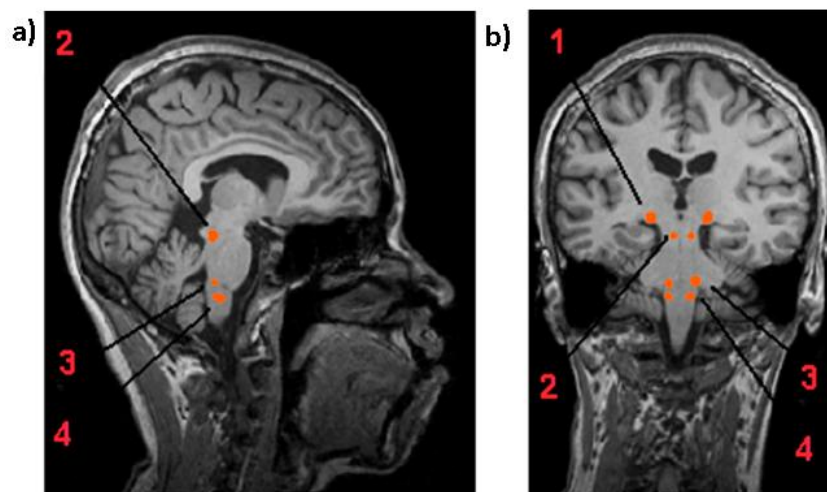


**Fig. 16; Figure illustrates positions of activated structures in brainstem obtained after statistical analysis (threshold:  $p < 0.001$  uncorrected). Positions were superimposed on anatomical image. In sagittal plane (a) positions of IC (1), SOC (3) and CN (4) are demonstrated. Coronal plane (b) illustrates IC (1), SOC (3), CN (4) and MGB (5).**

Using the positions of activated voxels it was possible to characterize time courses within auditory cortex. Periodical curves were obtained in block design experiment as a response of the acoustic stimulus for non-gated measurements, gated with and without correction (Fig.17). To get desired temporal information, first voxel was defined (coordinates). Then raw signal was extracted. In case of gated measurements it was necessary to pay attention on variable TR and their correction. Data is why in this case raw data was corrected using linear regressor. Presented time courses showed different behavior for different measurements and they correspond to results obtained through statistical analysis. In all cases the highest amplitude and quite symmetrical shape were found for gated measurements with correction. Curves for non-gated measurements were also symmetrical however the amplitude was lower. In case of gated measurements without any correction amplitude was much lower and in addition symmetrical shape was distorted.

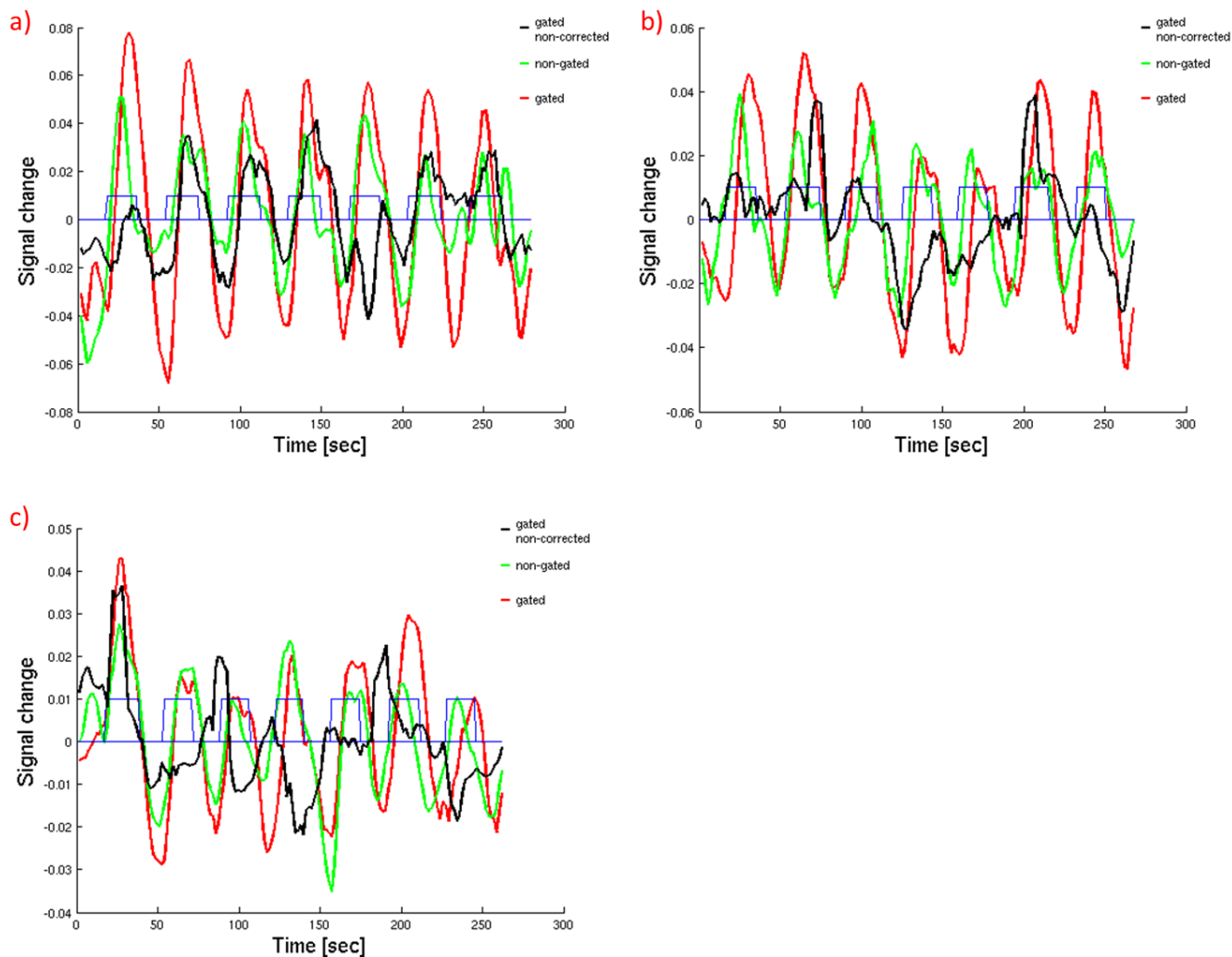


**Fig. 17; BOLD response function for local maximum corresponding area of auditory cortex for three different subjects (a ,b, c) and for non-gated measurements (green) , gated with ( red) and without corrections (black). Blue rectangles correspond to block design.**

## 4.2. OPTIMIZATION THE TECHNICAL PARAMETERS

This section is divided into four parts which contains the results from the method presented in the Chapter 3.2.2 concerning optimization the technical parameters.

### 4.2.1 NUMBER OF SLICES

For the experiment with 32 and 10 slices (Chapter 3.2.2.1) auditory cortex was activated in all individuals with the threshold of  $p < 0.001$  uncorrected. Higher mean t-values in auditory cortex were acquired for music stimuli than for tones ( $16.2 \pm 1.4$  and  $8.3 \pm 3.2$ , respectively).

In experiment with 32 slices, only three brainstem nuclei were visible: one located in SOC and two in IC (10% detectability). No activations were found in MGB, nuclei of LL and CN. Results are presented in Table 3. For the second experiment, activation was found in 10 nuclei (33%). No activation was found in SOC. There are some asymmetric responses for auditory cortex localized in left and right hemisphere; however it is not a rule that one side is more activated than the other. It seems to be randomized effect across the volunteers.

**Tab. 3; Table illustrates mean t-values and number of activated structures along auditory pathway (right and left hemispheres) for two kind of experiments with 32 and 10 slices. Obtained with the threshold of  $p < 0.001$  uncorrected for three volunteers.**

| Brain Region | 32 slices   |            | 10 slices   |             |
|--------------|-------------|------------|-------------|-------------|
|              | Right       | Left       | Right       | Left        |
| AC           | 10.93 (3/3) | 9.93 (3/3) | 12.49 (3/3) | 10.31 (3/3) |
| MGB          | -           | -          | 3.75 (1/3)  | -           |
| IC           | 7.47 (2/3)  | -          | 4.12 (1/3)  | 4.74 (2/3)  |
| Nuclei of LL | -           | -          | 5.18 (1/3)  | 3.40 (2/3)  |
| SOC          | 3.69 (1/3)  | -          | -           | -           |
| CN           | -           | -          | 3.80 (1/3)  | 4.30 (2/3)  |

### 4.2.2 RESOLUTION

Introduction to this part of the results was presented in Chapter 3.2.2.2. For the experiment with two different resolutions response to music was detected in all individuals in the right and left auditory cortex (AC). The t-values for local maxima in AC were: 13.68 and 14.67

respectively for first and second experiment. Structures corresponding with regions of brainstem were identified on the basis of the anatomical atlases. Threshold of  $p < 0.001$  uncorrected was used to count the number of active nuclei from the right and left hemispheres. Examples of t maps for standard statistical analysis are presented in the Figure 18 for both kinds of experiments.

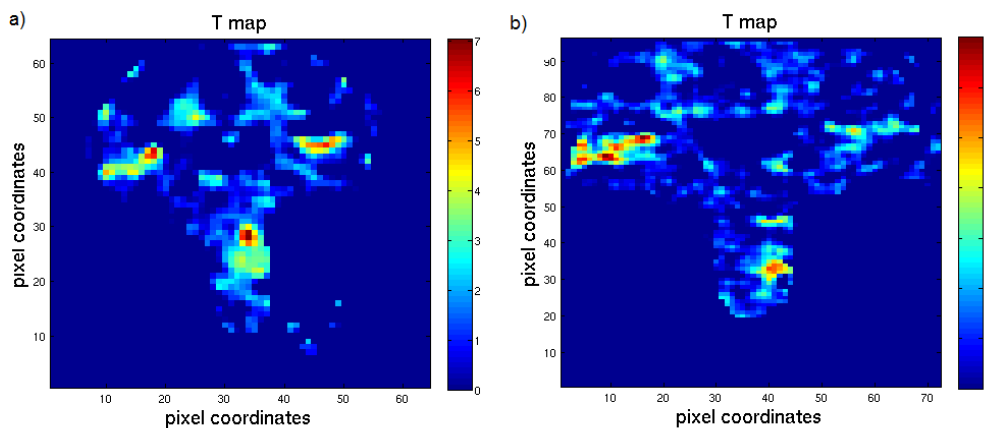


**Fig. 18; T maps for standard analysis for 1st experiment (2.5 mm) (a) and 2nd one (1,7 mm) (b). Examples of t maps are presented for one subject.**

All of the structures in auditory pathway were visualized partially: MGB in first and second experiment was detected in 25% and 19% of subjects respectively, inferior colliculi in 38% (first experiment) and 81% (second experiment), nuclei of lateral lemniscus in 56% and 25% for first and second experiment respectively. For cochlear nuclei in first and second experiment the percentage of detectability was 75% and 56% respectively and for superior olivary complex 44% (first experiment) and 6% (second experiment) in standard SPM analysis. Numbers of activated structures in standard analysis are presented in Table 4.

**Tab. 4;** Table shows the number of activated brainstem structures which were detected after standard analysis in two experiments: 1st with lower resolution (2.5 mm) and 2nd one with higher resolution (1.7 mm). Results presented are for 8 subjects.

| Brain Region | 1 <sup>st</sup> experiment |       | 2 <sup>nd</sup> experiment |       |
|--------------|----------------------------|-------|----------------------------|-------|
|              | Right                      | Left  | Right                      | Left  |
| MGB          | 2/8                        | 2/8   | 2/8                        | 1/8   |
| IC           | 8/8                        | 5/8   | 2/8                        | 4/8   |
| Nuclei of LL | 5/8                        | 4/8   | 1/8                        | 3/8   |
| SOC          | 3/8                        | 4/8   | 1/8                        | 0/8   |
| CN           | 6/8                        | 6/8   | 4/8                        | 5/8   |
| Mean         | 24/40                      | 21/40 | 10/40                      | 13/40 |

### 4.2.3 MONAURAL STIMULATION

Auditory cortex for the experiment with monaural stimulation (right and left ear stimulation) was activated in both hemispheres with threshold  $p < 0.001$  uncorrected. For all of the subjects, response in auditory cortex was stronger in the hemisphere contralateral to the stimulated ear (Tab.5). Right ear stimulation caused a significant activation of the right CN; the mean t-value was two times higher for the right than for the left CN. However, left IC and MGB responded more strongly than their right side counterparts. At the level of CN, response to left ear stimulation was essentially mirror symmetric to the response to right one, that is, the left sounds elicited a strong activation in the left CN and a weak activation in the right CN. There was no activation in superior olivary complex. Figure 19 and 20 present the mean t-values for both right and left ear stimulation.



**Tab. 5; Mean t-values and their standard deviations for AC, MGB, IC and CN (right and left hemispheres) for right ear and left ear stimulation (three volunteers).**

| Brain Region | Right ear stimulation |          | Left ear stimulation |          |
|--------------|-----------------------|----------|----------------------|----------|
|              | Right                 | Left     | Right                | Left     |
| AC           | 10.4±3.5              | 12.7±6.0 | 18.3±2.1             | 10.8±3.7 |
| MGB          | 2.9±1.1               | 4.8±2.9  | 3.9±2.4              | 2.3±3.1  |
| IC           | 2.0±1.4               | 3.7±1.4  | 4.3±1.7              | 2.8±2.7  |
| CN           | 3.7±1.8               | 1.7±2.2  | 1.9±2.4              | 4.1±2.1  |

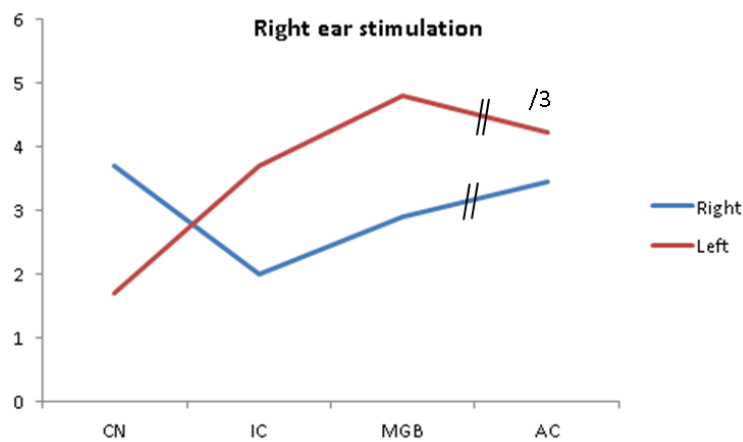


**Fig. 19; Graph is showing decomposition of t- values for auditory pathway (right ear stimulation). Real t-value for auditory cortex was divided by three to enhance better visualization of the results.**

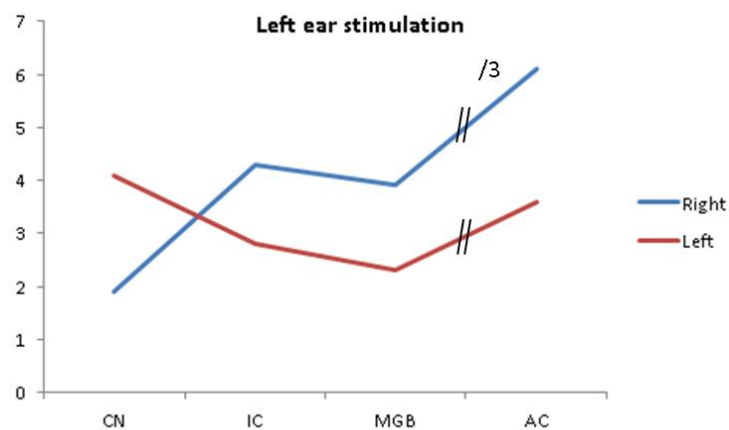


**Fig. 20; Graph is showing decomposition of t- values for auditory pathway (left ear stimulation). Real t-value for auditory cortex was divided by three to enhance better visualization of the results.**

#### 4.2.4 fMRI ACTIVATION IN RELATION TO SOUND INTENSITY

In this section, auditory pathway was examined with different amplitudes of presented stimuli. Results are presented in Table 6. The activation level in response to the music stimulation was higher in both cases for the standard amplitude of sound which was adapted by the subjects. In both cases, mean t-values for right hemisphere was significantly higher. The highest difference between t-values from normal and reduced sound amplitude was shown for the right side, rock music and the smallest for left side (classical music).

**Tab. 6; Mean t-values and their standard deviations for experiments with different sound amplitude: normal and reduced. Results are presented for two different auditory stimuli (music: rock and classical) and for 13 volunteers.**

| Side       | Rock music |          | Classical music |          |
|------------|------------|----------|-----------------|----------|
|            | normal     | reduced  | normal          | reduced  |
| Right Side | 15.1±5.9   | 12.9±3.2 | 13.3±3.3        | 12.2±4.5 |
| Left Side  | 14.5±5.0   | 12.6±4.4 | 11.9±3.9        | 11.6±6.1 |

### 4.3. FUNCTIONAL CONNECTION IN AUDITORY PATHWAY

Materials and methods for the results presented below are included in Chapter 3.2.3. The aim of the study was to investigate the auditory pathway using analysis of functional connectivity, which can describe the connections between functionally related regions. First conventional analysis was performed to identify local maximum in the region of auditory cortex, which in the next step was used for further analysis

#### *Conventional functional block design analysis*

Cortical auditory structures in the right and left hemispheres were detected in all 10 experiments with a threshold of  $p < 0.001$  uncorrected. Coordinates of local maxima in the region of auditory cortex for both hemispheres are presented in the Table 7. The mean values for both hemispheres and all kinds of auditory stimuli are presented in Table 8. Looking at the mean t-values higher activation rate was presented for rock music and for the right hemisphere, however comparing the results for each subject separately it was seen interindividual dependence.

**Tab. 7; Table presents coordinates corresponding region of right and left auditory cortex (local maximum) identified in standard t-test analysis (10 sessions: 5/rock music, 5/classical music).**

| Nr. | Rock music       |                 | Classical music  |                 |
|-----|------------------|-----------------|------------------|-----------------|
|     | Right<br>[x y z] | Left<br>[x y z] | Right<br>[x y z] | Left<br>[x y z] |
| 1.  | 55 9 33          | -53 10 36       | 58 10 36         | -56 10 30       |
| 2.  | 49 2 18          | -47 -2 18       | 49 6 19          | -47 -3 15       |
| 3.  | 52 4 21          | -50 4 21        | 52 4 21          | -53 4 21        |
| 4.  | 48 8 19          | -51 3 26        | 48 8 19          | -51 9 28        |
| 5.  | 46 14 2          | -53 -1 7        | 43 17 2          | -56 -1 7        |
| 6.  | 49 5 34          | -44 -9 30       | 49 4 31          | -47 -11 33      |
| 7.  | 43 10 26         | -50 -6 36       | 43 10 26         | -50 -7 33       |
| 8.  | 52 17 12         | -47 11 18       | 52 17 12         | -47 8 18        |

**Tab. 8; Table presents mean T values for right and left auditory cortex identified after rock and classical music stimulation.**

| Nr.                  | Rock music (t-values) |                 | Classical music (t-values) |                 |
|----------------------|-----------------------|-----------------|----------------------------|-----------------|
|                      | Right                 | Left            | Right                      | Left            |
| 1.                   | 18.80                 | 14.45           | 17.05                      | 15.08           |
| 2.                   | 17.25                 | 16.20           | 16.93                      | 16.06           |
| 3.                   | 27.61                 | 25.40           | 16.61                      | 20.36           |
| 4.                   | 12.68                 | 14.81           | 12.14                      | 12.72           |
| 5.                   | 25.85                 | 29.06           | 12.33                      | 12.60           |
| 6.                   | 20.20                 | 14.99           | 18.16                      | 13.05           |
| 7.                   | 27.39                 | 23.22           | 25.31                      | 17.65           |
| 8.                   | 19.33                 | 10.22           | 10.69                      | 13.68           |
| <b>Mean t-values</b> | <b>21.1±5.3</b>       | <b>18.5±6.5</b> | <b>16.2±4.6</b>            | <b>15.2±2.8</b> |

Subcortical auditory activation was examined in the following structures: cochlear nucleus (CN), superior olivary complex (SOC), nuclei of the lateral lemniscus (nuclei of LL), inferior colliculi (IC) and medial geniculate body (MGB). In Table 9 the number of identified subcortical activations is displayed in the left column. Figure 21 shows typical t-maps and reference time course of the seed voxel for one subject.

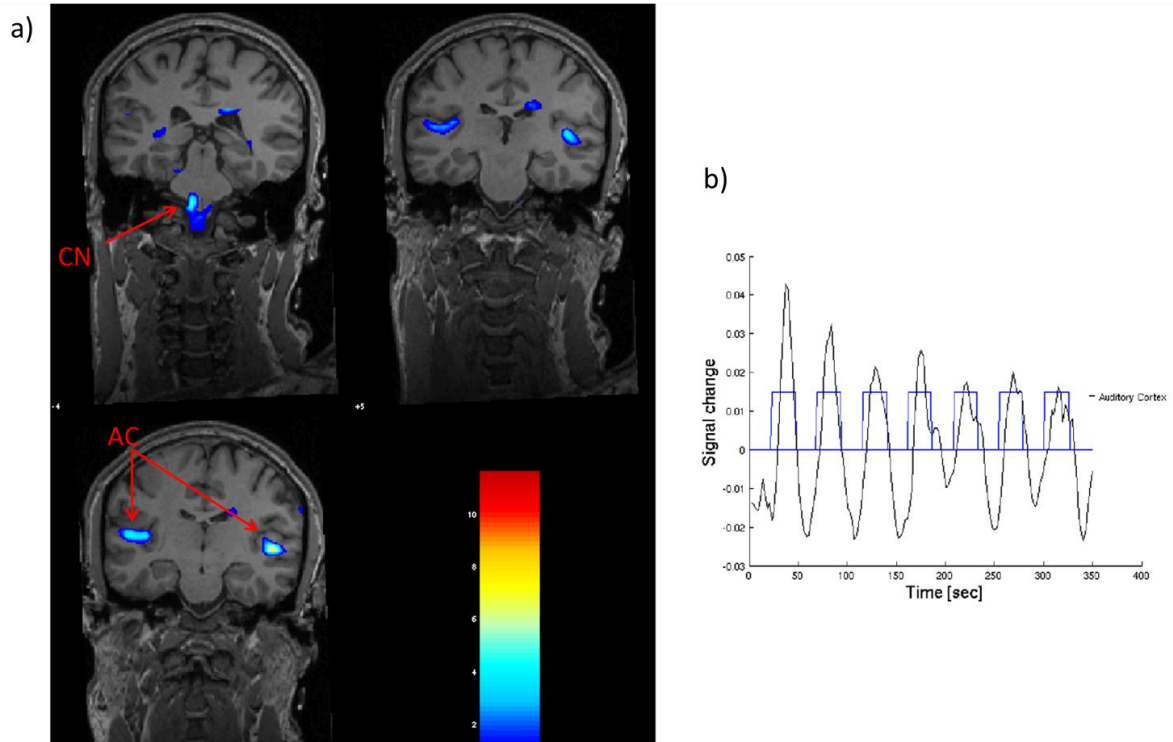


**Fig. 21;** T maps in coronal plane for auditory cortex and the brainstem (a). Reference time course for individual subject from auditory cortex (b).

**Tab. 9;** Numbers of detectable activations in brainstem area found in two kinds of analysis (standard one, using hemodynamic response function (HRF) and additional using auditory cortex signal (analysis of functional connections).

| Brain Region | Using HRF         |        |                   |        | Using AC signal   |        |                   |        |
|--------------|-------------------|--------|-------------------|--------|-------------------|--------|-------------------|--------|
|              | R (mean t-values) |        | L (mean t-values) |        | R (mean t-values) |        | L (mean t-values) |        |
| IC           | 4                 | (4.86) | 3                 | (5.21) | 10                | (5.21) | 9                 | (5.33) |
| Nuclei of LL | 1                 | (3.22) | 2                 | (3.56) | 4                 | (3.97) | 5                 | (4.56) |
| SOC          | 1                 | (3.86) | -                 |        | 4                 | (4.01) | 5                 | (3.67) |
| CN           | 3                 | (4.77) | 3                 | (4.23) | 5                 | (5.16) | 7                 | (4.76) |
| MGB          | 2                 | (5.01) | -                 |        | 5                 | (5.65) | 5                 | (4.23) |

#### *Analysis of functional connections*

In this analysis activations localized in subcortical areas were found in all 10 experiments (rock and classical music stimuli) with a threshold of  $p < 0.001$ . Figure 22 demonstrates activation maps after additional analysis, the time course of the seed region which is visualized together with time courses of activated brainstem structure and time course from other region of white matter. In Table 9 the number of detectable subcortical activations is

displayed in the right column. Visualization of the brainstem nuclei after analysis of functional connections is demonstrated in Figure 23.

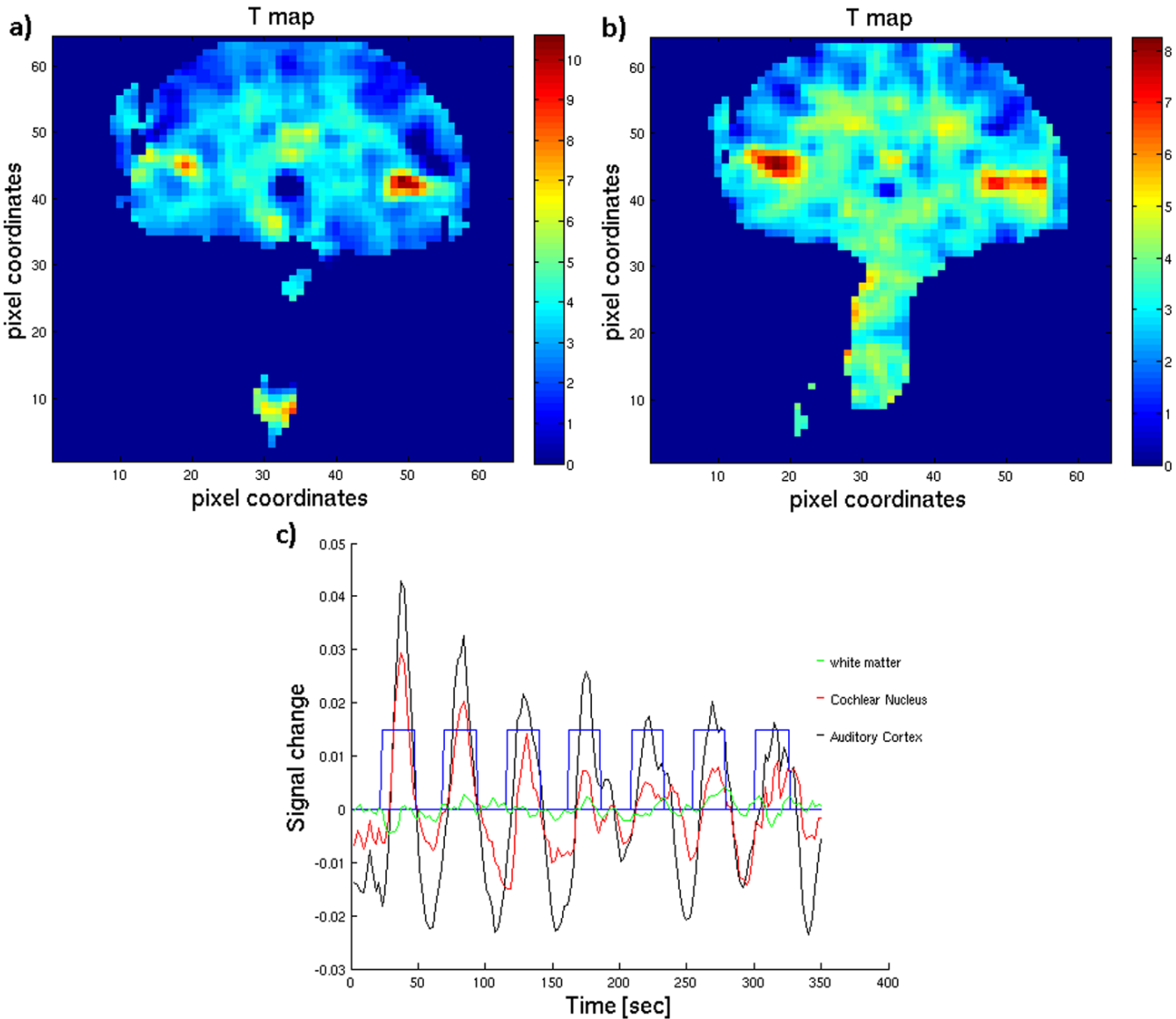


**Fig. 22;** Figure shows t maps in coronal plane after functional connectivity analysis for a slice through auditory cortex (a) and the brainstem (b). Reference time course is presented for individual subject from auditory cortex, time courses from positions corresponding region of brainstem (right hemisphere) and other white matter localization (c).

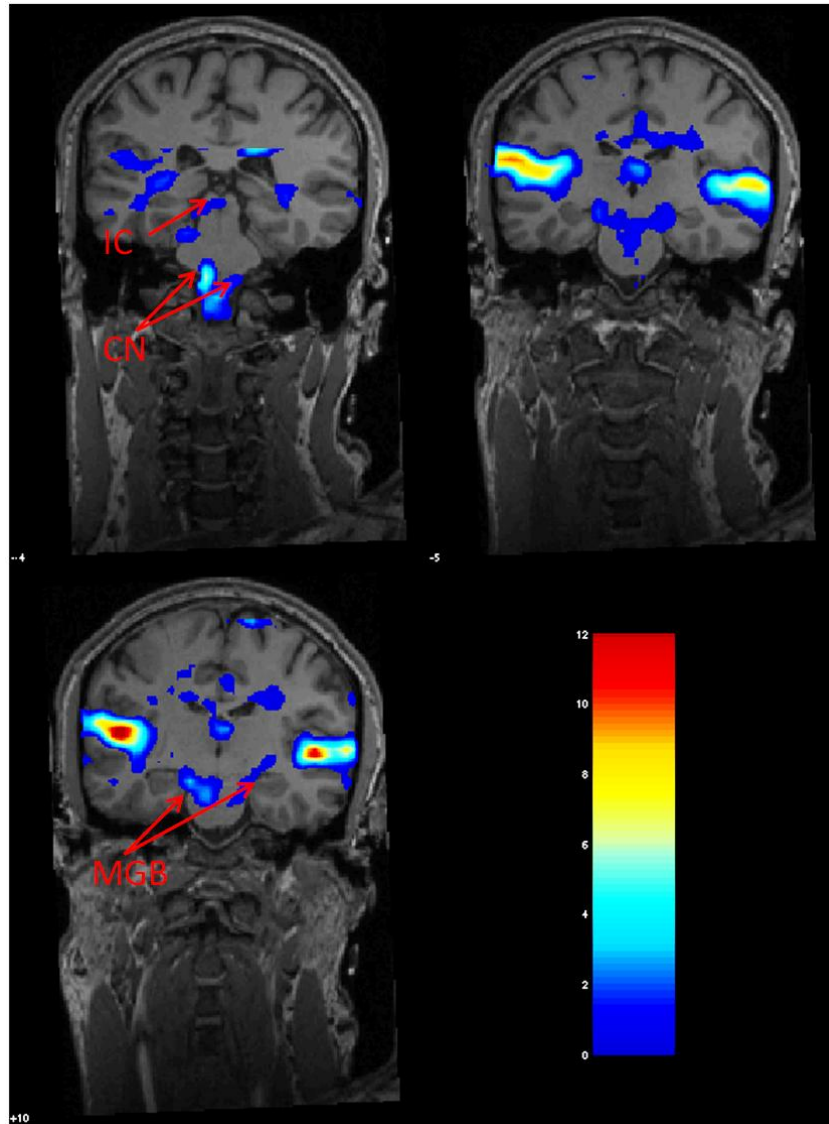


**Fig. 23; T maps in coronal plane after analysis of functional connections for the slices through auditory cortex and the brainstem. Figure illustrates localization of IC, CN (right and left) and MGB (right and left).**

#### 4.4. INFLUENCE OF WHITE MATTER CORRECTION ON VISUALIZATION OF AUDITORY PATHWAY

The aim of this chapter was to investigate the human auditory pathway, using a supplementary step in statistical analysis to improve the results. Signal from white matter was used as an additional regressor in statistical analysis. Introduction to this part was described in Chapter 3.2.4. The activation produced by the binaural music conditions was found in cortical and subcortical areas with the threshold of  $p < 0.001$  uncorrected. A single subject's analysis revealed that auditory cortex was significantly activated in all individuals for three analyses: single regressor (TR), single regressor (WM) and two regressors (TR, WM) with the threshold  $p < 0.001$  uncorrected. However the t-values for analysis with single regressor (WM) were more than two times smaller in comparison with the other two. For analysis without any regressor detectability of auditory cortex was 92%. Brainstem nuclei were not detected in analysis without any regressor and single regressor (WM).

For subcortical structures the detection rate was only 51% for analysis without WM (i.e. only one regressor, TR) correction compared to 87% for analysis with WM correction (i.e. using two regressors both TR and WM). Table 10 presents the t value statistics for the whole auditory pathway obtained during all analyses. It is evident that the statistical analysis that used WM as a regressor had a much higher detection rate than the statistical analysis without it.

**Tab. 10; Table presents results of mean t-values and number of detected subcortical structures (right and left hemispheres) from four different data analyses (24 volunteers).**

| Brain Region | Without Regressors |            | Single Regressor (TR) |             | Single Regressor (WM) |            | Two Regressors (TR and WM) |             |
|--------------|--------------------|------------|-----------------------|-------------|-----------------------|------------|----------------------------|-------------|
|              | Right              | Right      | Right                 | Left        | Right                 | Left       | Right                      | Left        |
| AC           | 4.6(22/24)         | 4.6(22/24) | 11.0(24/24)           | 12.6(24/24) | 5.3(24/24)            | 5.2(24/24) | 18.4(24/24)                | 15.3(24/24) |
| MGB          | -                  | -          | 3.5(14/24)            | 3.2(14/24)  | -                     | -          | 4.1(21/24)                 | 4.5(22/24)  |
| IC           | -                  | -          | 3.8(15/24)            | 3.6(15/24)  | -                     | -          | 5.6(24/24)                 | 5.3(24/24)  |
| SOC          | -                  | -          | 1.5(8/24)             | 2.3(8/24)   | -                     | -          | 3.0(15/24)                 | 3.0(16/24)  |
| CN           | -                  | -          | 3.5(12/24)            | 3.2(12/24)  | -                     | -          | 3.8 (24/24)                | 4.0 (23/24) |



## 4.5. CHIRP STIMULI

Below are presented the results from new chirp stimulus which was described in Chapter 3.2.5. The activation produced by the binaural chirp conditions was found in cortical and subcortical areas with the threshold of  $p < 0.001$  uncorrected. A single subject's analysis showed that auditory cortex was significantly activated in all individuals.

**Tab. 11; Numbers of activations and their mean t values with standard deviations (10 subjects).**

| Brain Region | Chirp                    |           |                         |           |
|--------------|--------------------------|-----------|-------------------------|-----------|
|              | Right<br>(mean t-values) |           | Left<br>(mean t-values) |           |
| AC           | 10                       | (6.9±2.5) | 10                      | (5.8±1.9) |
| MGB          | 10                       | (4.7±0.8) | 10                      | (5.0±0.9) |
| IC           | 10                       | (4.3±0.9) | 10                      | (5.0±0.9) |
| CN           | 10                       | (5.1±2.0) | 9                       | (5.1±1.2) |

The detection rate for subcortical structures was almost 100%. Table 11 indicates the number of positions and peak activation t-values of significantly activated regions included the ACs (auditory cortex), MGBs (medial geniculate body), ICs (inferior colliculi), and the CNs (cochlear nucleus) on both sides of the brain. Mean t values for AC were 6.9 for right side and for the left 5.8, for MGB right side 4.7, left side 5.0, for IC were 4.3 (right side), 5.0 (left side), and for CN were 5.1 and 5.1 respectively for right and left side. Figure 24 presents the localization of activated structures in auditory pathway.

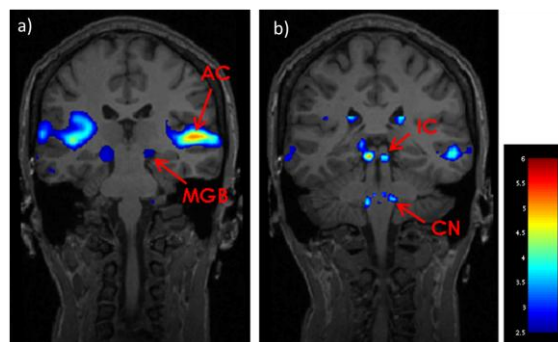


**Fig. 24; Localizations of auditory pathway for single subject: auditory cortex and medial geniculate body for right and left side (a), inferior colliculi and cochlear nucleus for right and left (b)  $p < 0.001$  uncorrected).**

#### 4.6. EFFECTS OF DIFFERENT TYPES OF AUDITORY STIMULI

Introduction to this section is described in Chapter 3.2.6. The activation in the auditory cortex in response to the various stimuli such as music (rock and classical), syllables and chirp stimuli was detected in all individuals in right and left hemisphere. Graph (Fig.25) corresponds to the Table 12; it presents the mean t-values for different stimuli. Classical music had the highest t-values both in the right and left hemisphere. T-values for rock music and syllables were comparable. Only t-values for chirp stimuli were more than two times smaller. Activation maps showed distinct foci of changes, in variable location across different sound stimulations distributed along primary auditory cortex (Fig.26). Values in the Table 13 correspond to presented t-maps. It was also shown that cluster size was the biggest for classical music (both hemispheres), and the smallest for chirp stimuli. Subcortical auditory activation was successfully visualized. The t-values are shown in Table 14 and comparable between different auditory stimuli (mean t-values: rock music 5.4, classical 4.8, syllables 4.8 and chirp 5.4). In case of brainstem structures the mean t-values are presented in the on the graph (Fig. 27) which corresponds to Table 15. The highest detection rate was observed for chirp stimuli (almost 100%), for rock music was 87%, in case of classical music detectability was 73% and for syllables 80%. Figures 28 and 29 presents the anatomical location of CN and IC achieved after chirp stimulation.

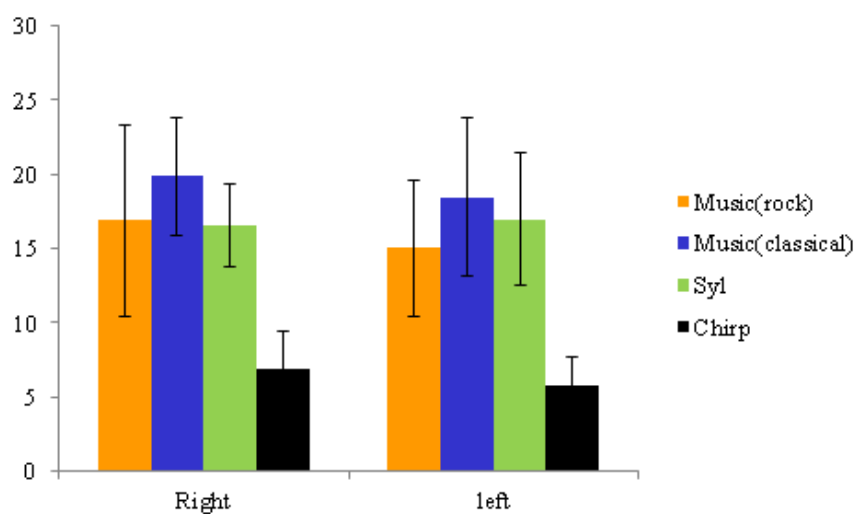


**Fig. 25; Mean t-values for different auditory stimuli, graph corresponds to the t-values from the Table 11.**

**Tab. 12; Mean t-values (10 subjects) presented for different auditory stimulation.**

| Side         | Rock music<br>(t-values) | Classical music<br>(t-values) | Syllables<br>(t-values) | Chirp<br>(t-values) |
|--------------|--------------------------|-------------------------------|-------------------------|---------------------|
| <b>Right</b> | 16.89±6.42               | 19.88±4.00                    | 16.59±2.75              | 6.95±2.46           |
| <b>Left</b>  | 15.06±4.59               | 18.46±5.32                    | 16.99±4.50              | 5.78±1.93           |

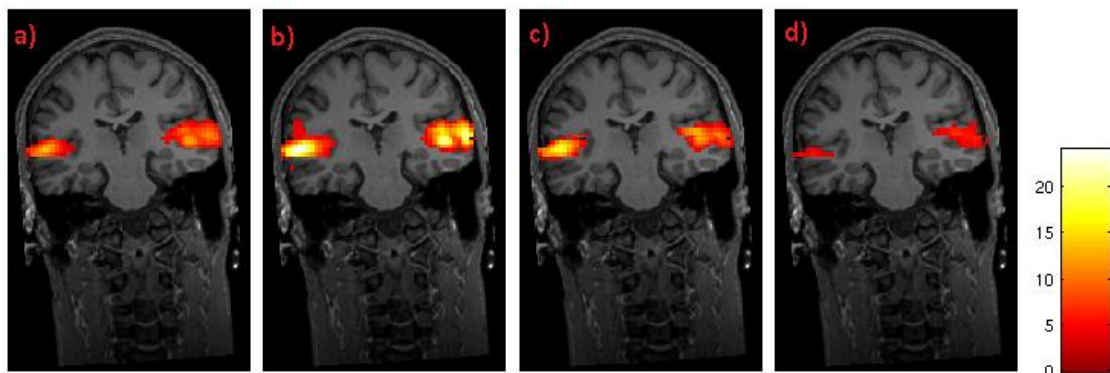


**Fig. 26; T maps with the threshold of  $p < 0.001$  (one subject) presents auditory cortex after stimulation of rock (a) and classical (b) music, syllables (c) and chirp (d).**

**Tab. 13; Maximal t-values for different type of stimuli and the size of the cluster. Table corresponds to Figure 19 (one subject).**

| Side         | Rock music<br>(max t-value,<br>cluster size) | Classical music<br>(max t-value,<br>cluster size) | Syllables<br>(max t-value,<br>cluster size) | Chirp<br>(max t-value,<br>cluster size) |
|--------------|--|---|---|---|
| <b>Right</b> | 12.7 (565)                                   | 21.5 (675)  | 8.2 (548)                                   | 7.6 (291)                               |
| <b>Left</b>  | 14.1 (290)                                   | 24.0 (450)  | 18.9 (320)                                  | 5.5 (57)                                |

**Tab. 14; Mean t-values for brainstem nuclei, different stimuli.**

| Stimuli         | MGB<br>(mean t-value) |         | IC<br>(mean t-value) |         | CN<br>(mean t-value) |         |
|-----------------|-----------------------|---------|----------------------|---------|----------------------|---------|
|                 | Right                 | Left    | Right                | Left    | Right                | Left    |
| Rock music      | 6.2±1.2               | 6.6±2.2 | 5.7±2.4              | 5.1±1.0 | 4.5±1.0              | 4.4±0.3 |
| Classical music | 4.6±2.2               | 5.1±1.8 | 4.6±1.1              | 6.1±2.2 | 4.5±1.3              | 3.8±0.7 |
| Syllables       | 5.6±1.5               | 4.1±1.7 | 4.8±3.1              | 4.1±2.9 | 5.1±2.2              | 5.2±3.0 |
| Chirp           | 7.0±0.8               | 5.8±0.9 | 4.3±0.9              | 5.0±0.9 | 5.1±2.0              | 5.1±1.2 |

**Tab. 15; Number of activated brainstem nuclei after different sound stimulation.**

| Stimuli         | MGB   |       | IC    |       | CN    |      |
|-----------------|-------|-------|-------|-------|-------|------|
|                 | Right | Left  | Right | Left  | Right | Left |
| Rock music      | 9/10  | 9/10  | 8/10  | 9/10  | 9/10  | 8/10 |
| Classical music | 8/10  | 8/10  | 8/10  | 7/10  | 7/10  | 6/10 |
| Syllables       | 8/10  | 9/10  | 7/10  | 8/10  | 8/10  | 8/10 |
| Chirp           | 10/10 | 10/10 | 10/10 | 10/10 | 10/10 | 9/10 |

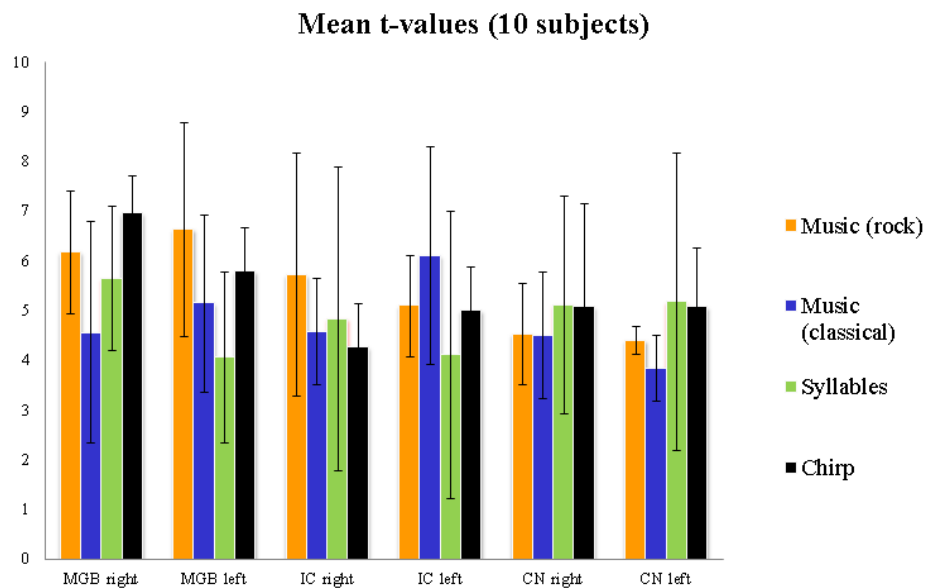


**Fig. 27; Graph presents mean t-values for different nuclei and stimuli.**

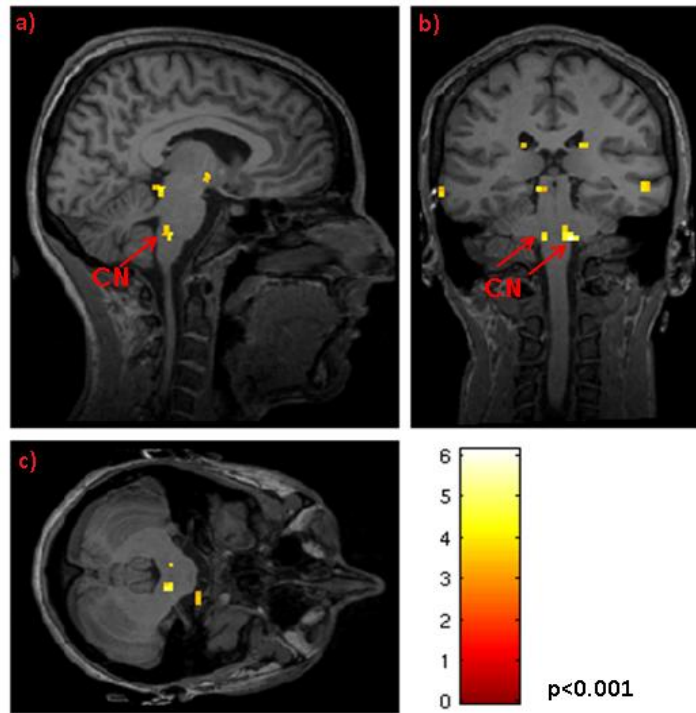


Fig. 28; T-maps illustrates cochlear nucleus (chirp stimuli) in different planes: sagittal (a), coronal (b) and axial (c).

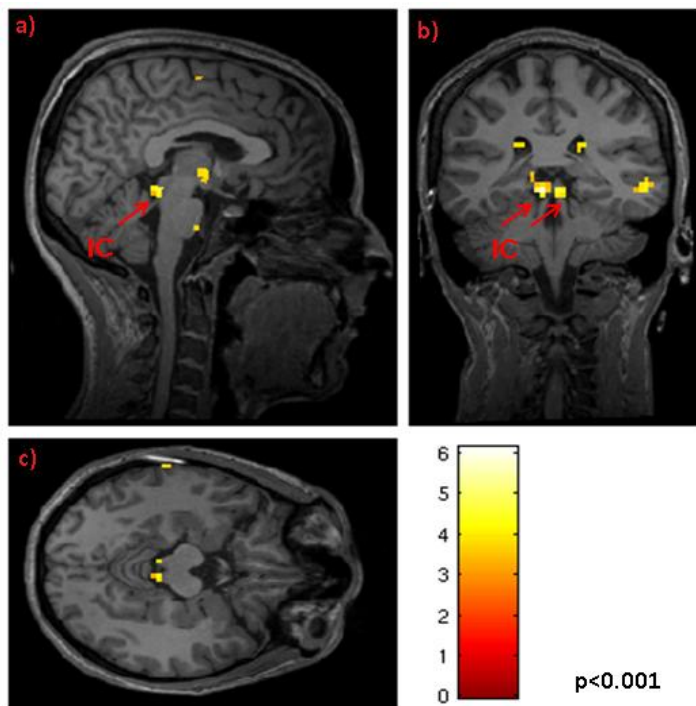


Fig. 29; T-maps illustrates inferior colliculi (chirp) in different planes: sagittal (a), coronal (b) and axial (c).

#### 4.7. INTERINDIVIDUAL STABILITY OF BRAINSTEM POSITIONS

Within this chapter I wanted to inspect the stability of individual activated positions within a group of healthy subjects and compare the coordinates of activated nuclei with previous studies and anatomical atlases. Methods part is included in Chapter 3.2.7.

The activation produced by the binaural music conditions was found in cortical and subcortical areas with the threshold of  $p < 0.001$  uncorrected. A single subject's analysis revealed that auditory cortex was significantly activated in all individuals for both analyses (with one and two regressors). But for subcortical structures the detection rate was only 51% for analysis without WM (i.e. only one regressor, TR) correction compare to 88% for analysis with WM correction (i.e. using two regressors both TR and WM). Table 16 presents the t value statistics for the whole auditory pathway obtained during analysis with one and two regressors.

Table 17 indicates the location and peak activation t-values for significantly activated regions including the MGBs, ICs, SOCs and the CNs on both sides of the brain. The locations of activated regions are compared with the previous by reported results. The variation of the peak positions found for subcortical structures was no more than 2mm.

**Tab. 16; Mean t-values for four statistical analyses and the number of positions that were found.**

| Brain Region | Single Regressor (TR) |             | Two Regressors (TR and WM) |                    |
|--------------|-----------------------|-------------|----------------------------|--------------------|
|              | Right                 | Left        | Right                      | Left               |
| AC           | 11.0(24/24)           | 12.6(24/24) | <b>18.4(24/24)</b>         | <b>15.3(24/24)</b> |
| MGB          | 3.5(14/24)            | 3.2(14/24)  | <b>4.1(21/24)</b>          | <b>4.5(22/24)</b>  |
| IC           | 3.8(15/24)            | 3.6(15/24)  | <b>5.6(24/24)</b>          | <b>5.3(24/24)</b>  |
| SOC          | 1.5(8/24)             | 2.3(8/24)   | <b>3.0(15/24)</b>          | <b>3.0(16/24)</b>  |
| CN           | 3.5(12/24)            | 3.2(12/24)  | <b>3.8 (24/24)</b>         | <b>4.0 (23/24)</b> |

Results from two overlay ROIs: CN and SOC showed that just for one person activation in left side for both ROIs was not found. CN was not identified just for one subject (left side), activation in SOC was not found for nine subjects (right side) and for the left side eight subjects. However, in case of these two nuclei, we were able to localize also additional maxima. For CN second maximum was found in five subjects (right side) and in three (left side), SOC in four volunteers just in the right side. The t-values were lower in comparison to the first maximum in the range of 0.66. Variation of the peak positions found for this second maximum was no more than 2 mm.

**Tab. 17;MNI coordinates of auditory activation. Average positions from our results of cortical and subcortical regions are presented for eight subjects (left and right hemispheres), their standard deviations and mean t-values (single subject analysis). Table presents also results from previous reported studies.**

| <b>Brain Region</b> |                   | <b>X</b><br>[mm] | <b>Y</b><br>[mm] | <b>Z</b><br>[mm] | <b>mean t- value</b> | <b>X</b><br>[mm] | <b>Y</b><br>[mm] | <b>Z</b><br>[mm] | <b>mean t- value</b> |
|---------------------|-------------------|------------------|------------------|------------------|----------------------|------------------|------------------|------------------|----------------------|
| <b>MGB</b>          | [59]              | -17              | -26              | -5               | 5.49                 | 15               | -26              | -2               | 4.81                 |
|                     | [60]              | -17              | -24              | -2               | -                    | 17               | -24              | -2               | -                    |
|                     | [61]              | -15              | -23              | -1               | -                    | -                | -                | -                | -                    |
|                     | [62]              | -14              | -26              | -8               | -                    | 12               | -24              | -8               | -                    |
|                     | [46]              | -17              | -26              | -2               | 4.01                 | 14               | -27              | 0                | 4.36                 |
|                     | [63]              | -15±3            | -25±1            | -9±2             | -                    | 17±1             | -25±1            | -7±1             | -                    |
|                     | <b>My results</b> | <b>-14±1</b>     | <b>-28±2</b>     | <b>-9±2</b>      | <b>4.5±1.9</b>       | <b>15±2</b>      | <b>-29±2</b>     | <b>-9±2</b>      | <b>4.1±1.4</b>       |
| <b>IC</b>           | [59]              | -5               | -38              | -6               | 8.42                 | 6                | -35              | -6               | 7.37                 |
|                     | [60]              | -6               | -33              | -11              | -                    | 6                | -33              | -11              | -                    |
|                     | [61]              | -                | -                | -                | -                    | 5                | -36              | -7               | -                    |
|                     | [62]              | -6               | -34              | -12              | -                    | 6                | -34              | -10              | -                    |
|                     | [44]              | -2               | -36              | -8               | 6.24                 | -                | -                | -                | -                    |
|                     | [46]              | 0                | -38              | -2               | 5.95                 | 3                | -36              | -8               | 7.91                 |
|                     | [63]              | -5±1             | -34±2            | -15±3            | -                    | 5±1              | -35±1            | -14±2            | -                    |
| <b>My results</b>   | <b>-5±2</b>       | <b>-36±2</b>     | <b>-11±2</b>     | <b>5.3±1.7</b>   | <b>6±2</b>           | <b>-35±2</b>     | <b>-11±2</b>     | <b>5.6±1.9</b>   |                      |
| <b>SOC</b>          | [60]              | -13              | -35              | -41              | -                    | 13               | -35              | -41              | -                    |
|                     | [46]              | -9               | -38              | -39              | 4.70                 | 8                | -38              | -41              | 2.81                 |
|                     | <b>My results</b> | <b>-8±2</b>      | <b>-37±2</b>     | <b>-41±1</b>     | <b>3.0±0.8</b>       | <b>9±2</b>       | <b>-37±2</b>     | <b>-41±1</b>     | <b>3.0±1.0</b>       |
| <b>CN</b>           | [60]              | -10              | -38              | -45              | -                    | 10               | -38              | -45              | -                    |
|                     | <b>My results</b> | <b>-7±2</b>      | <b>-39±1</b>     | <b>-45±1</b>     | <b>4.0±1.2</b>       | <b>9±1</b>       | <b>-39±2</b>     | <b>-45±1</b>     | <b>3.8±1.4</b>       |

## 5. DISCUSSION

---

The present study was designed to assess the visualization of cortical and subcortical regions within the auditory pathway using fMRI. Several methods are available for measuring activity in the brainstem by using fMRI [43, 45, 64], however, this is still methodological challenge. Many authors have tried to solve the difficulties in order to better visualize these regions [38, 65], with some success. Despite these current solutions, there remains a wide range of possibilities to further improve the data analysis to obtain more satisfactory results and use in the future as a clinical routine. In presented study, supplementary approaches in order to achieve satisfactory and stable results were applied.

### 5.1. OPTIMIZATION THE TECHNICAL PARAMETERS

fMRI images can indeed visualize a variety of functions related with brain functions, but only with appropriate fMRI sequence, right technical parameters, good design of the experiment or stimuli. Optimization of parameters in terms of number of slices, resolution and auditory stimuli is important to obtain the desired results. I proposed some modification to check possibility to improve the results.

First advantage was using 10 slices instead of 32. The influence of reduced number of slices was clearly visible through significantly higher detection rate for brainstem nuclei. Whole brain measurement (32 slices, each 3.2 mm thickness) gave maximal 20% detectability of brainstem nuclei, but for experiment with reduced number of slices (10 slices, 2.5 mm thickness) detectability was 53%. The reason for these results was variability of the heart rate which gave a bigger influence on volumes with 32 slices because of longer acquisition time.

Within the experiments with different resolution (Chapter 4.2.2) obtained higher detectability for experiment with lower resolution (2.5 mm) compare with higher (1.7 mm), 56% and 29% respectively. For the first experiment detection of inferior colliculi and cochlear nucleus were seen more frequently (81% and 75% respectively) than the rest of the structures. Most likely, IC ( $6 \times 6 \times 4 \text{ mm}^3$ ) and CN ( $3 \times 3 \times 7 \text{ mm}^3$ ) were seen more repeatable in the experiment with the lower resolution due to the bigger size comparing with the other nuclei (nucleus of LL and



SOC 2x2x5 mm<sup>3</sup>) [65]. Comparison between the experiments with different resolutions showed that for first one percentage of visible nuclei is higher, therefore I decided to use these parameters in the future experiments.

In the part of optimization the technical parameters, activation was determined in response to monaurally presented classical music (Chapter 4.2.3). For the auditory cortex, activation was strongest on the side contralateral to the stimulated ear; with activation level being about 1.2 times (right ear stimulation) and 1.7 (left ear stimulation) as high as those on the ipsilateral side. This is in good agreement with previous studies [46]. Similar ratios between right and left activation levels were observed for the IC and MGB also contralateral to the stimulated ear. This contralateral subcortical response patterns in MGB AND IC reflect similar contralateral preferences which have been found in the AC. However, activation to monaural stimulation in the CN was reported to be ipsilateral with ratio approximately 2.2 for right and left ear stimulation. These findings strongly suggest that auditory signals dominantly cross to the contralateral side above the level of CN [36, 48]. Figure 30 presents model of connections from the level of the stimulus delivery.

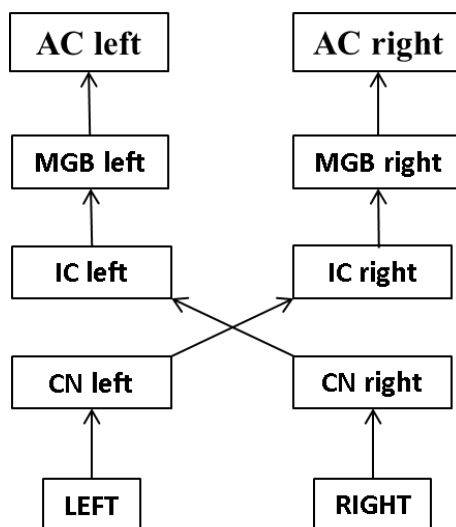


**Fig. 30; Model of connections to response of left and right ear stimulation.**

## **5.2. DATA EVALUATION**

fMRI data was collected using cardiac gated measurements. This method has been frequently used [36, 41, 50]. I proposed linear signal correction, because variations of repetition times in

each examination were small (less than 10%). Using TR as a regressor in statistical analysis, I was able to successfully visualize cortical and subcortical structures of auditory pathway [39, 65]. It was confirmed that this technique helps to minimize the movement artifacts resulting in higher detection rates in the regions of the brainstem (about 50% detectability compared with 0% for non-gated measurements). However, it was also observed that the activation of auditory cortex has been improved using gated measurements (an average of 2.4 times higher t-values) [66]. Up till now gated measurements were used only in case of subcortical parts of the brain [33, 35]. Nevertheless, these results showed that also for the cortical level, gated measurements became a key tool to give better results.

Up to now, information about functional connectivity involving cortical and subcortical structures is rare. The t-values after connectivity analysis compared to the standard t-test were slightly higher for the regions which were identified as brainstem structures [67, 68]. The functional connectivity analysis showed structures which were not accessible in standard analysis. Therefore functional connectivity analysis can help to identify subcortical regions of the auditory pathway in more detail. This approach showed that functional MR imaging reveals functional connectivity between cortical and subcortical regions. The investigation of functional connectivity in these areas combined with the cognitive tasks such as auditory stimuli can be an important tool for evaluating the auditory network in the human brain and improve the detection of brainstem nuclei, in healthy subjects and in patients with a variety of abnormalities in the auditory pathway such as acoustic neuroma. Such an investigation could show the distinctions in auditory pathway between healthy people and those with abnormalities. This could provide the important baseline for a comparison with auditory disorders and could help in future investigation and implantation.

The objective of this study was to improve also the post-processing step not only including analysis with repetition times as regressors but introduced an additional approach where we calculated the signal from white matter and used it as an additional regressor in statistical analysis. Acquired maps of t-values with only one nuisance regressor resulted in a lower detection rate for the whole auditory pathway than analyzing the data with two nuisance regressors. The presented approach helped to minimize global effects that are typically present during fMRI experiments, and which are likely to interfere with the detection of local BOLD signals [69]. Whilst the evaluation of the signal changes from the whole white matter has already been suggested by other investigators [56], this is the first report using WM as a nuisance regressor to visualize cortical and subcortical auditory areas.

### **5.3. EFFECT OF DIFFERENT AUDITORY STIMULATION**

Presented results demonstrated the capacity of fMRI to visualize auditory activation of human brainstem structures using the chirp stimulus. Many authors have tried to solve the difficulties connected with visualization of auditory pathway [44, 70]. However the detection rate of expected structures was not satisfactory. What is interesting, the new sound stimuli (chirp) showed t-values in auditory cortex almost 3 times lower compare with previous chapters. However, in the level of auditory brainstem it was observed that chirp detected almost 100% nuclei [71]. Presented study showed very high detection rate for visualization structures in brainstem compared with previous studies (80 %) [72]. It was the first time that a chirp stimulus was used in auditory fMRI to detect subcortical activations with satisfactory results. As was also observed for ABR, this stimulus gives us better results. The location of cortical and subcortical regions of auditory pathway corresponded well with the location of the particular activations in data of other fMRI studies within auditory pathway [46, 59, 73, 74]. Values of t parameter in activated areas in the region of auditory cortex allowed verifying which of the hemispheres had predominant significance in the executed experiment. For three stimuli (rock, classical music and chirp) predominant meaning had right hemisphere, for syllables left hemisphere. As we know the right hemisphere is particularly engaged in melodic perception and timbre (what is connected with presented music) however the left one appears to be specialized for both rhythm and access to musical semantic representations (identification and recognition of melodies). Classical music showed the highest t values in executed experiment. Why music gave us strongest activation? We know that listening to music is one of the most pleasurable human experiences. Enjoyment is strongly modulated by individual factors such as familiarity with the music, personality, current mood and taste. Rock music has melody and fast tempo and major mode and it is connected with happy emotions. Classical music showed lower tempo and minor mode, calmer, pleasant but in the other hand more relaxed (happy and sad emotions). Syllables were not pleasurable and even annoying. In individual analysis the situation is little bit different. Everything depends on music taste, habituation, and attention. These entire factors have big influence into visualization of auditory cortex. In case of brainstem up till now there is no information about influence of different types of stimuli. Thus why, these results showed almost comparable t-values for different types of sound. However, detectability was the highest for chirp stimuli what is related with special function of this new fMRI auditory stimulus.

#### **5.4. STABILITY OF PRESENTED METHOD**

The location of cortical and subcortical regions of the auditory pathway described here corresponds well with the locations reported in previous fMRI studies within the auditory pathway [46, 73-76]. In the current study, individual analysis of the main activation positions within brainstem was compared after normalization to a standard brain. It was found that the variation of the peak positions in the examined group of healthy volunteers was up to 2 mm. These small changes in peak positions between subjects provide stability of the presented method. The MNI coordinates match reasonably with the coordinates reported previously [44, 59, 60, 62, 63]. However, we observed also some differences in the peak positions between our study and previous one. For MGB the difference in z direction was about 8 mm [46, 61], and for IC x direction was about 5 mm and z direction about 9 mm [46].

In conclusion, within this study it was possible to visualize the auditory pathway using a block design paradigm with the application of different sound stimuli. Development of post-processing using TR and WM as regressors offers improvement in the visualization in both subcortical and auditory cortex structures in comparison with the other studies. The stability of the approach presented in this study proves that fMRI may play an important role in any routine MR examination. This method is efficient and can be easily used whilst additionally allowing the possibility to investigate the afferent auditory pathway in patients with hearing problems such as hearing loss or tinnitus. If a difference in fMRI activations between normal subjects and patients with hearing problems can be shown, then this method can be used for control or different treatment approaches. This could provide the important baseline for comparison with auditory disorders and could help in future investigation

## REFERENCES

---

1. Purcell, E. M., Torrey, H. C., & Pound, R. V. (1946). Resonance absorption by nuclear magnetic moments in a solid. *Phys. Rev.*, 69:37-38.
2. Bloch, F., Hansen, W.W., Packard, M.E. (1946) Nuclear induction. *Phys. Rev.* 69:127.
3. Lauterbur, P.C. (1973) Image Formation by Induced Local Interactions: Examples Employing Nuclear Magnetic resonance. *Nature* 242:190-191.
4. Mansfield, P., Grannell, P.K. (1973) NMR ‘diffractions’ in solids? *J. Phys. C* 6:L422-L426.
5. Mansfield, P. (1977) Multi-Planar Image Formation using NMR Spin Echoes. *J. Phys. C* 10: L55-L58.
6. Mansfield, P., Pykett, I.L. (1978) Biological and Medical Imaging by NMR. *J. Magn. Reson.* 29:355-373.
7. Jones, R.A, Brookes, J.A, Moonen Ch.T.W. (2001) Ultra –fast MRI. *Oxford University Press* 4:93-108.
8. Jezzard, P., Matthews, P.M., Smith, S.M. (2001) Functional MRI: An Introduction to Methods. *Oxford University Press*.
9. Press, W.A, Brewer, A.A., Dougherty, R.F., Wade. A.R., Wandell, B.A. (2001) Visual areas and spatial summation in human visual cortex. *Vision Res.*41:1321-1332.
10. Sanders, J.A., Lewine, J.D., Orrison, W.W. (1996) Comparison of Primary Motor Cortex Localization Using Functional Magnetic Resonance Imaging and Magnetoencephalography. *Hum. Brain Mapp.* 4:47-57.
11. Hickok, G., K. Okada & J.T. Serences. (2009) Area spt in the human planum temporale supports sensory-motor integration for speech processing. *J. Neurophysiol.* 101:2725–2732.
12. Koelsch, S. et al. (2006) Investigating emotion with music: an fMRI study. *Hum. Brain Mapp.* 27, 239–250.
13. Reber, P.J., Wong, E.C., Buxton, R.B. (2002) Comparing the brain areas supporting nondeclarative categorization and recognition memory. *Brain Res Cogn Brain Res.* 14(2):245-57.
14. Koelsch, S., Fritz, T., Schluz, K., Alsop, D., Schlaug, G. (2005) Adults and children processing music: an fMRI study. *Neuroimage* 25:1068–1076.

15. Borsook, D., Becerra, L.R. (2006) Breaking down the barriers: fMRI applications in pain, analgesia and analgesics. *Mol Pain*. 2:30.
16. Mitterschiffthaler, M.T., Ettinger, U., Mehta, M.A., Mataix-Cols, D., Williams, S.C. (2006) Applications of functional magnetic resonance imaging in psychiatry. *J Magn Reson Imaging* 23(6):851-61.
17. Detre, J.A. (2004) fMRI: applications in epilepsy. *Epilepsia* 4:26-31.
18. Hellera, S.L., Heiera, L.A, Wattsa, R. et al. (2005). Evidence of cerebral reorganization following perinatal stroke demonstrated with fMRI and DTI tractography. *J of Clinical Imaging* 29:283-287.
19. Medina, L.S., et al. (2005) Seizure disorders: Functional MR imaging for diagnostic evaluation and surgical treatment – prospective study. *Radiology* 236, 247-53.
20. Ogawa, S., Lee, T., Nayak, A.S., Glynn, P. (1990) Oxygenation-sensitive contrast in magnetic resonance imaging of rodent brain at high magnetic fields. *Magnetic Resonance in Medicine* 14:68-78.
21. Ogawa, S., Lee T.M., Barrere, B. (1993) The sensitivity of magnetic resonance image signals of a rat brain to changes in the cerebral venous blood oxygenation. *Magnetic Resonance in Medicine* 29:205-210.
22. Ogawa, S., Menon, R.S., Kim, S.G. & Ugurbil, K.(1998) On the characteristics of functional magnetic resonance imaging of the brain. *A. Rev. Biophys. Biomol. Struci.* 27:447–474.
23. *Stippich*, (2007) ;<http://www.fmrib.ox.ac.uk/education/fmri/introduction-to-fmri/what-does-fmri-measure>
24. <http://products.cochlearamericas.com/hearing-two-ears>
25. Buckner, R.L., Bandettini, P.A., O’Craven, K.M., et al. (1997) Detection of cortical activation during averaged single trials of a cognitive task using functional magnetic resonance imaging. *Proc. Natl. Acad. Sci. USA* 93:14878–14883.
26. Strainer, J.C., Ulmer, J.L., Yetkin, F.Z., Haughton, V.M., Daniels, D.L., Millen, S.J. (1997) Functional MR of the primary auditory cortex: an analysis of pure tone activation and tone discrimination. *Am J Neuroradiol* 18:601-610.
27. Wessinger, C., Tian, B., VanMeter, J.W., Platenberg, R.C., Pekar, J., Rauschecker, J.P. (1997) Hierarchical processing within human auditory cortex examined with fMRI. *Soc. Neurosci, Abstr.* 23:2073

28. Bernal, B. and Altman, N. R. (2001) Auditory Functional MR Imaging. *American Journal of Roentgenology* 176:1009-1015.
29. Eden, G.F., Joseph, J.E., Brown, H.E., Brown, C.P., Yeffiro, T.A. (1999) Utilizing hemodynamic delay and dispersion to detect fMRI signal change without auditory interference: the behavior interleaved gradients technique. *Magnetic Resonance in Medicine* 41:13-20.
30. Talvage, T.M., Edminster, W.B., Ledden, P.J., Wiesskoff, R.M. (1997) Quantitative assessment of auditory cortex response induced by imager acoustic noise. *Hum. Brain Mapp.* 7:79-88
31. Reuss, S. (2000) Introduction to the superior olivary complex. *Microscopy Research and Technique* 51(4):303-306.
32. Li, L., Yue, Q. (2002) auditory gating processes and binaural inhibition in the inferior colliculus. *Hearing Research* 168:98-109.
33. Daggi, M.S., Ingeholm, J.E., Haxby, J.V. (1999) Localization of cardiac induced signal change in fMRI. *NeuroImage* 9: 407-415.
34. Poncelet, B.P., Wedeen, V.J., Weisskoff, R.M., Cohen, M.S. (1992) Brain parenchyma motion: measurement with cine echo- planar MR imaging. *Radiology* 185(3): 645-51.
35. Guimaraes, A.R., Melcher, J.R., Talavage, T.M., et al. (1998) Imaging subcortical auditory activation in humans. *Human Brain Mapp.* 6:33-41.
36. Melcher, J.R., Sigalovsky, I.S., Guinan, J.J Jr., Levine, R.A. (2000). Lateralized tinnitus studied with functional magnetic resonance imaging: abnormal inferior colliculus activation. *J Neurophysiol* 83(2): 1058-1072.
37. Harms, M.P., Melcher, J.R. (2002) Sound repetition rate in the human auditory pathway: representations in the waveshape and amplitude of fMRI activation. *J Neurophysiol* 88:1433-1450.
38. Zhang, W.T., Mainero, C., Kumar, A., Wiggins, C.J., Benner, T., Purdon, P.L., Bolar, D.S., Kwong, K.K., Sorensen, A.G. (2006) Strategies for improving the detection of fMRI activation in trigeminal pathways with cardiac gating. *NeuroImage* 31:1506-12.
39. Ryn, M., Erb, M., Klose, U. (2009) Detection of fMRI activations after acoustic stimulation by correlation analysis. *IFMBE Proceedings* 25:193-196.
40. Birn, R.M., Bodurka, J., Bandettini, P.A. (2001) The efficacy of cardiac gating with variable TR correction in fMRI. *Proc. Intl. Soc. Mag. Reson. Med.*9:1219.

41. Hawley, M., Melcher, J.R., Fullerton, B.C. (2005) Effects of sound bandwidth on fMRI activation in human auditory brainstem nuclei. *Hear Res* 204(1-2): 101-110.
42. Rabe, K., Michael, N., et al. (2006) fMRI studies of sensitivity and habituation effects within the auditory cortex at 1.5T and 3T. *Journal of Magnetic Resonance Imaging*, 23(4):454-458.
43. Heßelmann, V., Wedekin, Ch., Kugel, H., Schulte, O., Krug, B., Klug, N., Lackner, K.J. (2001) Functional magnetic resonance imaging of human pontine auditory pathway. *Hear Res* 158:160-164.
44. Krumbholz, K., Schönwiesner, M., Rübsem, R., Zilles, K., Fink, G.R., von Cramon D.Y. (2005) Hierarchical processing of sound location and motion in the human brainstem and planum temporale. *Eur J Neurosci* 21(1):230-238.
45. Yetkin, F.Z., Roland, P.S., Mendelsohn, D.B., Purdy, P.D. (2004) Functional magnetic resonance imaging of activation in subcortical auditory pathway. *The Laryngoscope* 114:96-101.
46. Kovacs, S., Peeters, R., Smith, M., Dirk, De Ridder, Paul van Hecke, Sunaert, S. (2006) Activation of cortical and subcortical auditory structures at 3T by means of functional magnetic resonance imaging paradigm suitable for clinical use. *Invest Radiol* 41:87-96.
47. Baumgart, F., Kaulisch, T., Tempelmann, C., Gaschler-Markefski, B., Tegeler, C., Schindler, F., (1998). Electrodynamical headphones and woofers for application in magnetic resonance imaging scanners. *Med. Phys.* 25:2068-2070.
48. Langers, D.R.M., van Dijk, P., Backes, W.H. (2005) Lateralization connectivity and plasticity in the human central auditory system. *NeuroImage* 28:490-499.
49. Jäncke L., Peters, M., Schlaug, G., Posse, S., Steinmetz, H., Müller-Gärtner, H. (1998) Differential magnetic resonance signal change in human sensorimotor cortex to finger movements of different rate of the dominant and subdominant hand. *Brain Res Cogn Brain Res* 6:279-284.
50. Sigalovsky, I.S., Melcher, J.R. (2006) Effects of sound level on fMRI activation in human brainstem, thalamic and cortical centers. *Hear Res* 215(1-2):67-76.
51. Stein, T., Moritz, C.H., Quigley, M., Cordes, D., Haughton, V., Meyerand, E. (2000) Functional connectivity in the thalamus and hippocampus studied with functional MR imaging. *Am J Neuroradiol* 21:1397-1401.



52. Hirsch, J.G., Rossmanith, C., Lowe, M.J., Gass, A. (2005) Extended analysis of functional connectivity using low frequency BOLD fluctuations (LFBF). *Proc. Intl. Soc. Mag. Reson. Med.* 13: 179.
53. Biswal, B., Yetkin, F.Z., Haughton, V.M., Hyde, J.S. (1995) Functional connectivity in the motor cortex of resting human brain using echo-planar MRI. *Magn. Res. Med.* 34:537–541.
54. Mullinger, K.J., Morgan, P.S., Auer, D.P., Bowtell, R.W. (2009) Functional connectivity of auditory and visual areas during rest and stimulus presentation. *Proc. Intl. Soc. Magn. Reson. Med.* 14:3261.
55. Van de Ven, V.G., Formisano, E., Prvulovic, D., Roeder, C.H., Linden, D.E.J. (2004) Functional connectivity as revealed by spatial independent component analysis of fMRI measurements during rest. *Human Brain Mapp.* 22:165-178.
56. Spence, J.S., Carmack, P.S., Gunst, R.F., Schucany, W.R., Woodward, W.A., Haley, R.W. (2006) Using a white matter reference to remove the dependency of global signal on experimental conditions in SPECT analyses. *NeuroImage* 32:49-53.
57. Tsuchitani, C. (1983) Physiology of the auditory system in bases of auditory brainstem evoked responses. E. J. Moore(Ed): Grune and Stratton, New York.
58. Elberling, C., Don, M. (2008) Auditory brainstem responses to a chirp stimulus designed from derived-band latencies in normal-hearing subjects. *J Acoust Soc Am.* 124(5):3022-37.
59. Smith, M., Kovacs, S., de Ridder, D., Peeters, R., van Hecke, P., Sunaert, S. (2007) Lateralization of functional magnetic resonance imaging (fMRI) activation in the auditory pathway of patients with lateralized tinnitus. *Neuroradiology* 49: 669-679.
60. Mühlau, M., Rauschecker, J.P., Oestreicher, E., Gaser, C., Röttinger, M., Wohlschäger, A.M., Simon, F., Etgen, T., Conrad, B., Sander, D. (2006) Structural brain changes in tinnitus. *Cereb. Cortex* 16(9):1283-1288.
61. Landgrebe, M., Langguth, B., Rosengarth, K., Braun, S., Koch, A., Kleinjung, T., May, A., de Ridder D., Hajak, G. (2009) Structural brain changes in tinnitus: Grey matter decrease in auditory and non-auditory brain areas. *NeuroImage* 46(1): 213-218.
62. Overath, T., Cusack, R., Kumar, S., Kriegstein, K., Warren, J.D., Grube, M., Carlyon, R.P., Griffiths, T.D. (2007) An information theoretic characterization of auditory encoding. *Plos Biology* 5(11): 2723-2732.

63. Kriegstein, K., Patterson, R.D., Griffiths, T.D. (2008) Task-Dependent modulation of medial geniculate body is behaviorally relevant for speech recognition. *Curr Biol.* 18(23-2):1855-1859.
64. Backes, W.H., van Dijk, P. (2002) Simultaneous sampling of event-related BOLD responses in auditory cortex and brainstem. *Magn Reson Med* 47(1):90-96.
65. Ryn, M., Erb, M., Klose, U. (2010) Method Development for Visualization of the Auditory Pathway Using fMRI. *Medizinische Physik* 10:173-175.
66. Ryn, M., Erb, M., Klose, U. (2012) Auditory cortex stimulation by fMRI using cardiac gated measurements. *Proceedings ESMRMB 2012* 325:245.
67. Ryn, M., Erb, M., Klose U. (2009) Detection of fMRI Activations After Acoustic Stimulation by Correlation Analysis. *IFMBE Proceedings* 25/II:193-196.
68. Ryn, M., Erb, M., Klose, U. (2010) Functional connectivity between structures in auditory pathway using fMRI technique. *Proc. Intl. Soc. Mag. Reson. Med.* 18:3490.
69. Desjardins, A.E., Kiehl K.A., Liddle P.F. (2001) Removal of confounding effects of global signal in functional MRI analyses. *NeuroImage* 13:751-758.
70. Hu, X., Tuong Huu Le, Parrish, T., Erhard, P. (1995) Retrospective estimation and correction of physiological fluctuation in functional MRI. *MRM* 34:201-211.
71. Ryn, M., Nunes, I., Rüttinger, L., Erb, M., Klose U. (2012) Visualization of auditory pathway by fMRI using chirp stimuli. *Proceedings ESMRMB 2012* 426: 326.
72. Ryn, M., Charyasz, E., Erb, M., Klose, U. (2011) An fMRI Investigation of Auditory Pathway Using Different Paradigms and Analysis. *IFMBE Proceedings* 34:57-60.
73. Belin, P., Yatorre, R.J, Hoge, R., Evans, A.C., Pike, B. (1999) Event-related fMRI of the auditory cortex. *NeuroImage* 10: 417-429.
74. di Salle, F., Formisano, E., Seifritz, E., Linden, D.E.J., Scheffler, K., Saulino, C., Tedeschi, G., Zanella, F.E., Pepino, A., Goebel, R., Marciano, E. ( 2001) Functional fields in human auditory cortex revealed by time-resolved fMRI without interference of EPI noise. *NeuroImage* 13:328-338.
75. Griffiths, T.D., Uppenkamp, S., Johnsrude, I., Josephs, O., Patterson, R.D. (2001) Encoding of the temporal regularity of sound in the human brainstem. *Nature Neuroscience* 4(6): 633-637.
76. Schönwiesner, M., Krumbholz, K., RübSamen, R., Fink, G.R., von Cramon, D.Y. (2007) Hemispheric asymmetry for auditory processing in the human auditory brainstem, thalamus and cortex. *Cereb Cortex* 17(2):492-499.

## ACKNOWLEDGMENTS

---

Completing a PhD has been truly a long journey, and I would not have been able to complete it without the aid and support of several people. First and foremost I would like to thank my supervisor Prof. Uwe Klose. It has been a privilege to have him as a mentor. Over few last years, he was encouraging me to finish my PhD thesis. I thank him for having made my PhD project an intellectual challenge and for having provided me with such an exceptional work environment. I would like to thank Dr. Micheal Erb and Bernd Kardatzki for knowing the answer to every technical question I have ever asked. I wish to thank also all my professors for the knowledge and helping me to develop a passion in science.

I wish to thank Franziska Hoesl for support in dealing with the administrative issues. The joy and enthusiasm she has. That was for me contagious and motivational, even during tough times. I thank to all our technical assistants: Mathias Röger, Albertine Stiens and Cornelia Veil. I thank my office mates: Grzegorz Chadzynski, Barbara Piotrowska, Paulina Palowska, Agata Zawadzka for bearing with me for so many hours. I especially thank Edyta Charyasz. Your patient and care have been a tremendous help for me, both personally and academically. Many thanks to my dear friends and colleagues for their trust and care.

Thanks to Promotionsstipendien nach dem Landesgraduiertenförderungsgesetz (LGFG) Eberhard Karls Universität Tübingen for financing my research.

I especially thank my family for their support in difficult moments. I hope that dealing with the long distance will at least bring them a little pride and much reassurance.

## **CURRICULUM VITAE**

---

Michalina Ryń

06.07.1984, Tychy, Poland

### **SCHOOL EDUCATION**

09/1991-06/1999

Primary School, Tychy, Poland

09/1999-06/2003

Stanislaw Wyspianski High School, Tychy, Poland

### **HIGHER EDUCATION**

10/2003-06/2006

Bachelor Studies, Department of Medical Physics,  
Faculty of Mathematics, Physics and Chemistry,  
University of Silesia, Katowice, Poland

10/2006 – 07/2008

Master Studies, Department of Medical Physics,  
Faculty of Mathematics, Physics and Chemistry,  
University of Silesia, Katowice, Poland

07/2007-12/2007

Erasmus Exchange Programme  
Eberhard Karls Universität Tübingen, Germany

Since 04/2008

PhD student (Dr. sc. hum.), Faculty of Medicine  
Eberhard Karls Universität Tübingen, Germany

## **PROFESSIONAL EXPERIENCE**

- 07/2005 - 07/2005  
Practical Training  
Department of Radiobiology, Wojewodzki Szpital  
Specjalistyczny Im. Prof. Jozefa Gasinskiego  
(Hospital), Tychy, Poland
- 09/2005 – 09/2005  
Practical Training  
Department of Anesthesiology and Intensive Care,  
Gornoslaskie Centrum Zdrowia Dziecka i Matki Im.  
Jana Pawla II (Hospital), Katowice, Poland
- 07/2007 – 12/2007  
Scientific Researcher  
Abteilung für Diagnostische und Interventionelle  
Neuroradiologie, Sektion Experimentelle  
Kernspinresonanz de ZNS Universitätsklinikum  
Tübingen, Germany
- 09/2008 – 10/2012  
Scientific Researcher  
Abteilung für Diagnostische und Interventionelle  
Neuroradiologie, Universitätsklinikum Tübingen,  
Germany
- 11/2012 – 12/2012  
Scientific Researcher  
Abteilung für Biomedizinische Magnetresonanz,  
Universitätsklinikum Tübingen, Germany

## PUBLICATIONS

1. Ryn M., Nunes I., Erb M., Rüttinger L., Klose U. Visualization of auditory pathway by fMRI using chirp stimuli. *Proceedings ESMRMB* (2012) 426 :326
2. Ryn M., Erb M., Klose U. Auditory cortex stimulation by fMRI using cardiac gated measurements. *Proceedings ESMRMB* (2012) 325: 245
3. Ryn M., Charyasz E., Erb M., Klose U. An fMRI Investigation of Auditory Pathway Using Different Paradigms and Analysis Procedures. *IFMBE Proceedings, Springer* (2011) 34: 57-60
4. Ryn M., Erb M., Klose U. Method Development for Visualization of the Auditory Pathway Using fMRI. *Medizinische Physik* (2010) 10: 173-175
5. Klimas A., Ryn M., Piotrowska B., Erb M., Klose U., Drzazga Z. Studies of the Human Auditory Pathway by Functional MRI and Brainstem Auditory Evoked Potentials. *Polish Journal of Environmental Studies* (2010) 1: 34-40
6. Ryn M., Erb M., Klose U. Functional connectivity between structures in auditory pathway using fMRI technique. *Proc. Intl. Soc. Mag. Reson. Med.* (2010) 18: 3490
7. Palowska P., Ryn M., Klose U., Drzazga Z. Analysis of BOLD signal in the brainstem during resting state and after continuous sound activation. *Proceedings XLII Polish Seminar on Nuclear Magnetic Resonance and Its Applications* (2009)
8. Ryn M., Piotrowska B., Erb M., Klose U. Aktivierungen im Hirnstamm bei akustischer Stimulation. *Neuroradiologie* (2009) up2date 1: 156
9. Ryn M., Erb M., Klose U. Detection of fMRI Activations After Acoustic Stimulation by Correlation Analysis. *IFMBE Proceedings* (2009) 25/II: 193-196

10. Ryn M., Piotrowska B., Gharabaghi A., Klose U. Darstellung der hörnervenkerne durch fMRI-messungen bei akustischer Stimulation. *RöFo* (2009) 181: 275

#### SCIENTIFIC PRESENTATIONS

1. Ryn M., Erb M., Klose U., Verbesserung von fMRI-Messungen des Auditorischen Kortexes durch Triggerung auf die Herzfunktion. 47.Jahrestagung der Deutschen Gesellschaft für Neuroradiologie, 11-13 Oct. 2012, Köln, Germany
2. Ryn M., Nunes I., Erb M., Rüttinger L., Klose U., Visualization of auditory pathway by fMRI using chirp stimuli. 29th Annual Scientific Meeting of ESMRMB, 4-6 Oct. 2012, Lisboa, Portugal
3. Ryn M., Erb M., Klose U., Auditory cortex stimulation by fMRI using cardiac gated measurements. 29th Annual Scientific Meeting of ESMRMB, 4-6 Oct. 2012, Lisboa, Portugal
4. Ryn M., Nunes I., Erb M., Rüttinger L., Klose U., Visualization of auditory pathway by fMRI using chirp stimuli. 43. Jahrestagung der Deutschen Gesellschaft für Medizinische Physik, 26-29 Sep. 2012, Jena, Germany
5. Ryn M., Erb M., Klose U., Stimulation with Chirp-pulses in fMRI measurements of the auditory pathway. International workshop "Magnetic Resonance Studies", 25-27 Jun. 2012, Oberschwarzenberg, Austria
6. Ryn M., Erb M., Klose U., Detection of fMRI activation in auditory pathway after sound stimulation. 1st International Workshop on Segregation and Integration in music and language, 24-25 Feb. 2012, Tübingen, Germany
7. Ryn M., Charyasz E., Erb M., Klose U., An fMRI Investigation of Auditory Pathway Using Different Paradigms and Analysis Procedures. 15. Nordic-Baltic Conference on Biomedical Engineering and Medical Physics, 14-17 Jun. 2011, Aalborg, Denmark

8. Ryn M., Erb M., Klose U., Intraindividual stability of activated cluster positions within cortical and subcortical structures of the auditory pathway. International workshop “Magnetic Resonance Studies”, 6-8 Jun. 2011, Trest, Czech Republic
9. Ryn M., Erb M., Klose U., Method Development for Visualization of the Auditory Pathway Using fMRI. 41. Jahrestagung der Deutschen Gesellschaft für Medizinische Physik, 29 Sep-02 Oct. 2010, Freiburg, Germany
10. Ryn M., Erb M., Klose U., Visualization of auditory pathway by fMRI. International workshop “Magnetic Resonance Studies”, 14-17 Jun. 2010, Oberjoch, Germany
11. Ryn M., Erb M., Klose U., Functional connectivity between structures in auditory pathway using fMRI technique. 18th Annual Scientific Meeting of ISMRM, 1-7 Mai. 2010, Stockholm, Sweden
12. Palowska P., Ryn M., Klose U., Drzazga Z., Analysis of BOLD signal in the brainstem during resting state and after continuous sound activation. XLII Polish Seminar on Nuclear Magnetic Resonance and Its Applications, 1-2 Dec. 2009, Krakow, Poland
13. Ryn M., Piotrowska B., Erb M., Klose U., Aktivierungen im Hirnstamm bei akustischer Stimulation. NeuroRAD-44 Jahrestagung der DGNR, 8-10 Oct. 2009, Köln, Germany
14. Ryn M., Erb M., Klose U., Detection of fMRI Activations After Acoustic Stimulation by Correlation Analysis. Medical Physics and Biomedical Engineering World Congress, 7-12 Sept. 2009, München, Germany
15. Ryn M., Erb M., Klose U., fMRI of the brainstem. International workshop “Magnetic Resonance Studies”, 5-6 Jun. 2009, Vienna, Austria



16. Ryn M., Piotrowska B., Gharabaghi A., Klose U., Darstellung der Hörnervenkerne durch fMRI-messungen bei akustischer Stimulation. Deutscher Röntgenkongress, 20-26 May 2009, Berlin, Germany